Check for updates

Solar RRL

WILEY VCH

Solar RRL

RESEARCH ARTICLE

Machine Learning-Assisted Novel Photovoltaic Optimization for Tailored Ultra-Thin CdTe-Based Solar Cells

Erman Cokduygulular[1] | Caglar Cetinkaya[2]

[1]Department of Engineering Sciences, Faculty of Engineering, Istanbul University-Cerrahpaşa, Istanbul, Türkiye | [2]Physics Department, Faculty of Science, Istanbul University, Istanbul, Türkiye

Correspondence: Caglar Cetinkaya (caglarcetinkaya@istanbul.edu.tr)

Received: 15 June 2025 | **Revised:** 25 July 2025 | **Accepted:** 20 August 2025

Keywords: artificial intelligence | CdTe solar cell | deep Q-learning | machine learning | photovoltaic optimization | reinforcement learning | transfer matrix method | ultra-thin CdTe

ABSTRACT

This study presents a machine learning-based design framework utilizing deep Q-learning (DQL) to optimize ultra-thin CdTe solar cells with active layer thicknesses ranging from 100 to 400 nm. By coupling the transfer matrix method for optical analysis with SCAPS-1D simulations for electrical modeling, the DQL agent effectively explored the complex parameter space, optimizing the thicknesses of all key layers, including SnO_2, CdS, CdTe, MoO_3, and Au. The DQL framework intelligently adjusted each layer based on electromagnetic wave propagation and absorption profiles, enhancing internal reflection and light trapping within sub-micron geometries. Even at extremely low absorber thicknesses (e.g., 100 nm), the optimized structures achieved high photovoltaic performance, with power conversion efficiencies up to 9.39% and J_{sc} values exceeding 11 mA/cm^2. At 400 nm, efficiency increased to 15.75% with J_{sc} of 20.86 mA/cm^2. These results demonstrate that efficient photon harvesting and carrier transport are achievable through full-stack optimization. External quantum efficiency and absorption spectra confirmed the integrated optical-electrical enhancement achieved by DQL. This work highlights the capabilities of reinforcement learning in high-dimensional solar cell design problems and provides a scalable approach for developing next-generation, lightweight, efficient, and material-conscious photovoltaic technologies.

1 | Introduction

Solar energy stands out as one of the most prominent representatives of green energy, relying on semiconductor systems that convert solar radiation into electrical power. These systems attract significant attention due to their environmentally friendly nature, low-cost production processes, and high-efficiency potential. In response to the rapidly increasing global energy demand, the need for clean and affordable energy sources is becoming increasingly critical. In this context, photovoltaic technologies enable the efficient and cost-effective conversion of solar photon energy into electricity. In the optical design of solar cells, artificial intelligence (AI) offers advanced solutions by accurately, rapidly, and efficiently calculating the optical properties of all layers, thereby maximizing photon harvesting efficiency. This capability introduces the potential to explore design spaces that are inaccessible through conventional methods. While the design of complex, multilayer optical thin-film systems has traditionally relied on human intuition, such approaches are often slow and inadequate in reaching optimal solutions [1].

Conventional approaches prove to be limited in terms of both efficiency and speed when exploring expansive design spaces, necessitating more systematic, innovative, and automated solutions. At this point, AI is revolutionizing solar cell design by rapidly and precisely analyzing the optical properties of multilayered systems. AI-assisted approaches not only enable performance optimization but can also be employed to establish an optimal

© 2025 Wiley-VCH GmbH.

balance between energy efficiency and transparency. Particularly in the wide spectral bands, the dispersion effects of materials become important, and AI-based models offer more accurate solutions by accounting for such optical variability [2]. Deep learning algorithms that enable the learning of Maxwell's equations offer significant advantages in deciphering the nonlinear relationships between structural parameters and optical performance across large datasets [3–6]. Deep learning not only surpasses existing performance boundaries but also emerges as a powerful tool for exploring new design domains [4, 7].

Recent advances in AI have significantly expanded its role in sustainable energy materials and photovoltaic research, particularly in the domains of material discovery, property prediction, and device-level optimization. For instance, deep learning models have been employed to accurately predict bandgap energies, defect tolerances, and structural stability in novel photovoltaic materials, accelerating the discovery of next-generation semiconductors beyond conventional screening approaches [8]. Furthermore, graph neural networks and inverse design strategies have been integrated to autonomously identify materials with optimal optoelectronic properties, significantly reducing the experimental burden and time required for validation [9]. Beyond material-level applications, AI-driven methods have also demonstrated remarkable success in simulating and optimizing full-device architectures by accounting for complex interdependencies between multiple performance metrics, such as power conversion efficiency (PCE), optical transmittance, and stability. Reinforcement learning (RL), in particular, has emerged as a powerful framework for navigating high-dimensional design spaces and balancing competing objectives in solar cell design [10]. These developments clearly illustrate the transformative potential of AI in advancing photovoltaic technologies, providing not only predictive insights but also prescriptive design pathways. The present study builds upon this momentum by applying a deep Q-learning (DQL)-based optimization framework to explore ultra-thin CdTe-based solar cell configurations in an integrated optical-electrical simulation environment.

Recent advancements have increasingly demonstrated the integration of machine learning (ML) techniques into solar cell research, particularly for performance optimization, prediction, and design refinement. Supervised learning models, such as support vector machines and multilayer perceptrons, have shown remarkable success in predicting photovoltaic parameters based on material and structural input features [11, 12]. These approaches enable rapid screening of candidate device configurations, bypassing time-intensive simulations. Moreover, convolutional neural networks and deep neural networks have been employed to analyze nonlinear relationships between input layer properties and resulting solar cell performance, achieving high prediction accuracy for open-circuit voltage (V_{oc}), short-circuit current density (J_{sc}), maximum power point (V_m, J_m), PCE, and fill factor (FF) [12]. In addition to predictive modeling, hybrid frameworks combining numerical simulations with ML algorithms have emerged as powerful tools for enhancing device design. For instance, integrated approaches utilizing SCAPS-1D with neural network regressors have enabled real-time performance prediction and parameter tuning for perovskite and CdTe-based solar cells [13]. More recently, RL and decision-tree-based algorithms have been adopted to identify optimal configurations in complex device architectures by evaluating multiple variables such as defect density, layer thickness, and doping levels [14]. These studies collectively underscore the growing relevance of ML in the solar energy field, aligning with the motivation and methodology of the present study, which introduces a DQL framework for the full-stack optimization of ultra-thin CdTe-based solar cells.

Unlike supervised and unsupervised learning techniques, RL provides a framework in which an agent learns optimal control within a dynamic environment based on reward feedback [15, 16]. RL is an approach in which an agent learns through experience which actions to take in order to maximize a numerical reward signal. Without being explicitly told which actions to perform, the agent must discover the most rewarding behaviors through trial and error. In this context, actions can influence not only immediate rewards but also future states and, consequently, long-term cumulative rewards. The trial-and-error exploration process and the mechanism of delayed rewards are among the fundamental distinguishing features of RL [2]. RL problems utilize Markov decision processes (MDPs) to define the interaction between an agent and its environment through the "state-action-reward" triplet. This framework represents the process in which agents interact with their environments by perceiving states, taking actions based on those states, and striving to achieve specific goals. As structures that concisely yet comprehensively incorporate fundamental elements such as perception, action, and objective, MDPs form the foundation of RL problems [2]. One of the key distinguishing features of RL is its systematic focus on computational problems that arise during interaction with the environment while pursuing long-term objectives [2]. In this context, the DQL algorithm, as a subfield of RL, effectively addresses RL problems by employing artificial neural networks to estimate Q-values in high-dimensional states and action spaces [17, 18].

Regarding photovoltaic technologies, cadmium telluride (CdTe), which possesses a direct bandgap of 1.5 eV and a high absorption coefficient on the order of 10^4 cm^{-1}, stands out due to its excellent light absorption capability [19]. CdTe-based thin-film solar cells can capture up to 90% of incident light with only a few microns of thickness and can be fabricated into large-area, uniform, and high-efficiency modules through various deposition techniques [1]. Typically exhibiting a polycrystalline structure, CdTe is employed in conjunction with a p-type CdTe absorber layer deposited on an n-type buffer layer, with cadmium sulfide (CdS) being the most commonly used material for the buffer layer [1].

Although the electronic properties of CdTe were discovered as early as 1947, its potential for photovoltaic performance was first discussed in 1956 [20, 21]. Initially demonstrating an efficiency of around 6% in the 1970s [22], CdTe technology has undergone significant advancements, recently achieving a record efficiency of 23.1% through the use of selenium and arsenic doping [23]. Today, CdTe modules dominate the thin-film photovoltaic market and have become one of the most commercially successful PV technologies [24, 25]. However, challenges such as limited global tellurium reserves (~47,000 tons) [26] and the relatively high tellurium requirement (~100 tons/GW) [27] constrain large-scale deployment. Material costs—especially for high-purity CdTe—and environmental concerns related to cadmium further

2367198x, 0, Downloaded from https://onlinelibrary.wiley.com/doi/10.1002/solr.202500455 by Cagla Cetinkaya - Istanbul University , Wiley Online Library on [02/09/2025]. See the Terms and Conditions (https://onlinelibrary.wiley.com/terms-and-conditions) on Wiley Online Library for rules of use; OA articles are governed by the applicable Creative Commons License

emphasize the need for material-efficient alternatives [28]. Consequently, reducing the thickness of the CdTe absorber layer has emerged as a critical strategy for alleviating material scarcity and minimizing environmental impact. While current devices typically employ CdTe layers with thicknesses ranging from 2 to 8 μm [29], the high absorption capability of CdTe permits further thickness reduction without significant performance loss [30]. Ultra-thin CdTe solar cells with absorber thicknesses below 1 μm [31] have demonstrated theoretical efficiencies of up to 93% photon absorption at a thickness of 1 μm [32]. Such designs not only maintain competitive performance but also offer advantages such as reduced material consumption, shorter production times, lower costs, and improved understanding of device physics, all while addressing sustainability concerns related to the use of tellurium and cadmium [33].

In recent years, experimental studies on ultra-thin CdTe solar cells have demonstrated consistency with theoretical simulations. For instance, Amin et al. [31] achieved an efficiency of 11.2% using a 0.6 μm-thick CdTe absorber layer on borosilicate glass [33]. Paudel and colleagues optimized the CdS window layer thickness and attained efficiencies of 8% and 11% with CdTe absorber layers of 0.25 and 0.5 μm, respectively, attributing the observed efficiency loss primarily to insufficient photon absorption [25, 33, 34]. While reports on CdTe solar cells with absorber layers thinner than 250 nm are rare in the literature, it has been suggested that high performance at such thicknesses may be achievable through careful control of the magnetron sputtering process [33]. Addressing concerns regarding the stability of ultra-thin structures, Paudel et al. [35]. conducted 1000 h accelerated lifetime tests on devices with absorber thicknesses ranging from 0.7 to 2.1 μm, observing no significant degradation in performance parameters. These findings indicate that reducing the thickness of the CdTe absorber layer does not negatively affect device stability [25].

For structures with the thinnest absorber layers, Lasieniak et al. successfully fabricated a solution-processed, sintered CdTe absorber with a thickness of 90 nm, achieving a PCE of 2.1% [36]. In terms of optimizing both PCE and absorber thickness, Plotnikov et al. achieved an 8% PCE using only a 0.25 μm-thick CdTe layer fabricated via sputtering [37]. Similarly, Paudel et al. also achieved 8% PCE with 0.25 μm-thick CdTe layers using the same sputtering technique [33]. The results of these studies, which represent some of the thinnest ultra-thin CdTe solar cells ever produced, demonstrate that magnetron sputtering is highly suitable for fabricating ultra-thin CdS/CdTe solar cells, particularly in terms of absorber thinness and photovoltaic performance. Although research on ultra-thin CdTe-based solar cells and the development of innovative device architectures have primarily focused on enhancing PCE, photon harvesting, and transmittance, these studies have also paid specific attention to whether the requirement for semitransparency is fulfilled in the infrared (IR) region.

In the present study, an innovative approach is proposed to optimize the optical and electrical performance of ultra-thin CdTe-based solar cells with an FTO/SnO_2/CdS/CdTe/MoO_3/Au architecture. The primary objective is to enhance device efficiency in solar cells with ultra-thin active layers ranging from 100 to 400 nm by maximizing photon harvesting through the application of a DQL algorithm. In this context, the DQL algorithm is employed not only to optimize the thickness of the active layer but also of all functional layers, including the window layer, electron transport layer (ETL), hole transport layer (HTL), and top contact. Through this holistic approach, the optical and electrical processes influencing device performance are assessed in an integrated manner. Furthermore, SCAPS-1D simulations are used to analyze the energy band diagrams and *J–V* characteristics of the devices, while optical transmittance and absorption spectra are calculated using the transfer matrix method (TMM) to elucidate the physical underpinnings of the DQL-driven optimization. Thus, this ML-assisted study presents a significant innovation by offering a faster and more efficient alternative to conventional methods for optimizing ultra-thin CdTe-based solar cells.

2 | Materials and Methods

This study aims to develop an innovative approach for designing ultra-thin CdTe-based solar cells by utilizing the DQL algorithm. The research primarily focuses on maximizing the optical and photovoltaic performance of CdTe-based cells with the thinnest possible active layer thickness (≤400 nm). The DQL-based ML algorithm developed for this purpose is designed to optimize the thickness of each layer in the ultra-thin CdTe solar cell architecture in accordance with specific optical and photovoltaic performance targets.

The main layers and material structure of the solar cell were designed based on the FTO/ SnO_2/CdS/CdTe/MoO_3/Au configuration, which is presented in detail in the *Solar Cell Architecture* section. The TMM was employed for optical calculations, while photovoltaic parameters and energy band diagrams were analyzed using the SCAPS-1D simulation software. The developed DQL algorithm enabled the simultaneous evaluation of optical properties (transmittance, absorption, and reflectance spectra) and photovoltaic performance (J_{ph}, band diagrams, and solar cell output parameters), thereby facilitating the identification of optimal ultra-thin CdTe-based solar cell designs. The ultra-thin CdTe solar cell architecture used in the study, along with the optical properties of the constituent materials and the optimization process performed using the DQL model, is schematically illustrated in Figure 1. Figure 1 includes: (a) the solar cell architecture, (b) the wavelength-dependent variations in the refractive index and extinction coefficient of the materials, and (c) the neural network architecture and training environment of the DQL model.

2.1 | Solar Cell Architecture

In the study, all ultra-thin CdTe-based solar cell architectures (Figure 1a) preferred fluoride-doped tin oxide (FTO) coated on a glass substrate as the bottom contact material. FTO is notable for its high electrical conductivity and optical transparency within the wavelength range effective under the AM1.5G solar spectrum. These properties enable the FTO layer to transmit sunlight into the device at maximum efficiency, facilitating the delivery of photons to the active region. In addition, a SnO_2 layer—distinguished by its wide optical bandgap, high transparency,

2367198x, 0, Downloaded from https://onlinelibrary.wiley.com/doi/10.1002/solr.202500455 by Cagla Cetinkaya - Istanbul University , Wiley Online Library on [02/09/2025]. See the Terms and Conditions (https://onlinelibrary.wiley.com/terms-and-conditions) on Wiley Online Library for rules of use; OA articles are governed by the applicable Creative Commons License

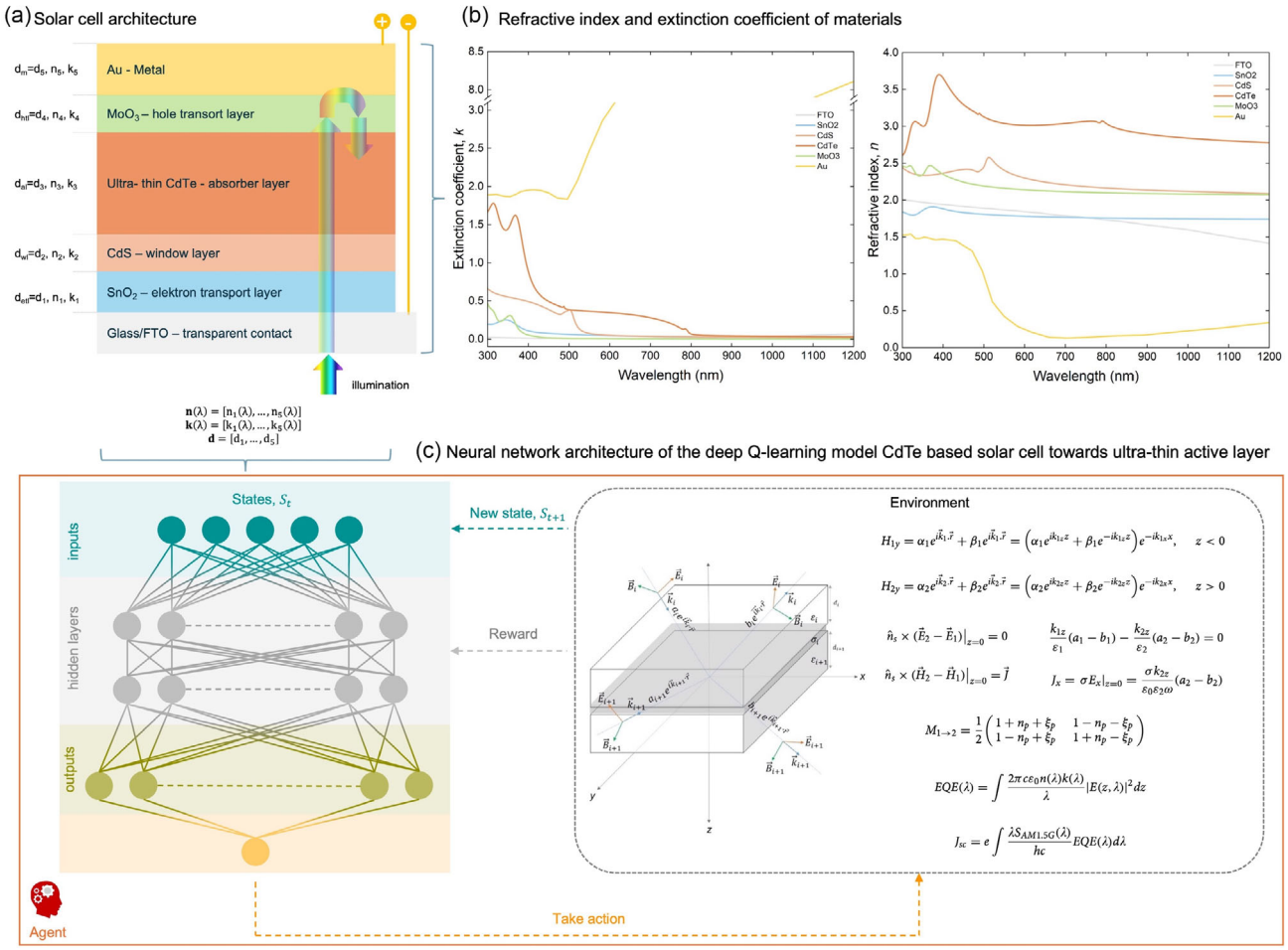


FIGURE 1 | (a) Architecture of the developed ultra-thin CdTe-based solar cell. (b) Wavelength-dependent refractive index and extinction coefficient of the materials. (c) The artificial neural network architecture of the DQL model was designed for the ultra-thin CdTe-based solar cell and the environment model used during the training process. The neural network evaluates new states and rewards at each step to optimize the layer thicknesses.

and excellent electrical conductivity—was deposited on top of the FTO to prevent the recombination of photogenerated charge carriers. The SnO_2 layer acts as a transparent transition medium, helping to form proper band alignment by mitigating structural leakage caused by voids at the bottom contact. Therefore, SnO_2 simultaneously functions as the ETL within the device.

To enhance the efficiency of this structure, an n-type CdS window layer was incorporated to facilitate the absorption of electromagnetic waves and promote the transfer of free electrons into the SnO_2 layer. CdS, an II-VI group compound semiconductor, is a promising material due to its n-type characteristics and a wide direct bandgap of 2.42 eV [38, 39]. CdS can exist in two distinct crystal structures—zinc blende (cubic phase) and wurtzite (hexagonal phase)—or as a mixture of both phases [38, 40, 41]. The active layer in the constructed solar cell architectures consists of an ultra-thin (≤400 nm) CdTe absorber layer, which is capable of generating a large number of electron–hole pairs to ensure high photovoltaic performance.

In addition to the majority carriers generated by photogeneration, the minority carriers are retained around the p–n junction region and collected more efficiently due to the effect of the internal electric field. Furthermore, a MoO_3 layer is added to the back surface of the structure as a back surface field to reduce recombination. Owing to its suitable work function and high p-type doping capability, MoO_3 facilitates the formation of ohmic contact and enables selective carrier transport by preventing photogenerated electrons from reaching the top contact [42]. At the same time, MoO_3 also serves as an HTL within the solar cell. Additionally, due to the high electron affinity of CdTe's band structure, ohmic contacts can be established with high work function metals. Therefore, Au metal contact was selected as the top electrode in the CdTe-based solar cell to enhance device performance [43].

2.2 | Calculating Optical and Photovoltaic Performances

The TMM, a widely used technique for multilayer optoelectronic structures that provides high accuracy, was employed to determine the optical properties of ultra-thin CdTe-based solar cells. TMM enables the calculation of optical properties such as reflectance, absorptance, and transmittance by analyzing the propagation of electromagnetic waves within the structure. The method has been shown to yield reliable results in both our previous studies and those of other research groups in the literature [44–47]. It is based on constructing transfer matrices that link the electric

2367198x, 0, Downloaded from https://onlinelibrary.wiley.com/doi/10.1002/solr.202500455 by Cagla Cetinkaya - Istanbul University , Wiley Online Library on [02/09/2025]. See the Terms and Conditions (https://onlinelibrary.wiley.com/terms-and-conditions) on Wiley Online Library for rules of use; OA articles are governed by the applicable Creative Commons License

and magnetic field components of the electromagnetic wave at the interfaces between the layers. Additionally, the propagation matrix enables the calculation of wave transmission across layers, allowing for detailed modeling of optical behavior. One of the main advantages of TMM is its ability to accurately evaluate the optical properties of solar cells that incorporate metal layers with varying conductivities alongside dielectric and semiconductor materials. This makes it particularly suitable for analyzing the optical performance of complex, multilayer solar cells that include combinations of dielectric, metallic, and semiconductor layers. Accordingly, in this study, the reflection, absorption, and transmittance characteristics of the designed ultra-thin CdTe-based solar cells were calculated and optimized using the TMM. Detailed optical analyses were thus conducted to enhance device performance by accounting for interlayer interactions. The computational methodology is presented in detail in our earlier publications that applied the TMM approach [47–51].

The photovoltaic performance analyses of ultra-thin CdTe-based solar cells were conducted using the SCAPS-1D simulation software. SCAPS-1D (Solar Cell Capacitance Simulator 1D) is a powerful tool specifically developed to analyze the electronic and optoelectronic performance of multilayer solar cell structures. This software enables detailed modeling of the electrical behavior between layers composed of different materials, the device characteristics, and the physical processes that influence overall device performance [52]. SCAPS-1D allows for the extraction of energy band diagrams by solving the band structure of the semiconductor layers. It also computes current density–voltage (J–V) characteristics, enabling detailed evaluation of key photovoltaic parameters such as V_{oc}, J_{sc}, V_m, J_m, PCE, and FF. This enables the comparative evaluation of the effects of different design parameters on device performance.

The basic computational principle of SCAPS-1D involves solving the Poisson equation and the charge carrier transport equations (drift-diffusion equations) to determine the spatial and energetic distribution of charge carriers in semiconductor devices. The software calculates the distribution of electrostatic potential using the Poisson equation while modeling the transport and recombination of charge carriers under the influence of an electric field, employing drift-diffusion equations. This approach reveals the electrical characteristics of the device. By analyzing the spatial variation of the electric field, carrier concentrations, and current densities within the solar cell, SCAPS-1D enables the derivation of reliable insights into the device's optoelectronic performance. In this study, the optimization and performance evaluation of ultra-thin CdTe-based solar cells were carried out through a comprehensive analysis based on band diagrams, J–V characteristics, and fundamental photovoltaic parameters obtained from SCAPS-1D simulations. In this way, the influence of material properties and layer thicknesses on photovoltaic performance was thoroughly examined during device design. The material parameters used in the simulations are presented in Table 1.

2.3 | Deep Q-Learning Strategy for Design of Ultra-Thin CdTe-Based Solar Cells

This study focuses on enhancing the photovoltaic performance of ultra-thin CdTe-based solar cells by utilizing DQL-based algorithms. The primary objective is to develop solar cell

TABLE 1 | Basic physical parameters and defect parameters of the materials used in SCAPS-1D simulations for the photovoltaic performance analysis of ultra-thin CdTe-based solar cells.

	CdTe	CdS	MoO_3	SnO_2	FTO
Bandgap (eV), E_g	1.45	2.4	3	3.5	3.6
Electron Affinity (eV), χ_e	3.9	4	2.5	4	4
Dielectric Permittivity (relative), ε	9.4	10	12.5	9	9
CB effective DOS (1/cm^3), N_c	8E = 17	2.2E + 18	2.2E + 18	4E + 18	2.2E + 18
VB effective DOS (1/cm^3), N_v	1.8E + 19	1.8E + 19	1.8E + 19	2E + 19	1.8E + 19
Electron thermal velocity (cm/s), $v_{e,\ t}$	–	1E + 07	1E + 07	–	1E + 07
Hole thermal velocity (cm/s), $v_{h,\ t}$	–	1E + 07	1E + 07	–	1E + 07
Electron mobility (cm^2/Vs), μ_e	320	100	25	100	20
Hole mobility (cm^2/Vs), μ_h	40	25	100	25	10
Shallow uniform donor N_D (1/cm^3)	0	1.1E + 18	0	1E + 18	1E + 18
Shallow uniform donor N_A (1/cm^3)	2E + 14	0	1E + 18	0	–
References	[53]	[54]	[55]	[56]	[57]
DEFECTS PARAMETERS					
Defect Density	1E + 15	1E + 17	1E + 15	1E + 15	1E + 15
Defect Energy Level (eV)	0.6	0.1	0.6	0.6	0.6
Type of Defect	Single donor	Single acceptor	Single acceptor	Single donor	Single donor
Capture Cross Section for Electrons (cm^{-2})	1E-14	1E-17	1E-15	2E-14	2E-14
Capture Cross Section for Holes (cm^{-2})	1E-14	1E-13	1E-15	2E-14	2E-14
References	[58]	[58]	[58]	[58]	[58]

2367198x, 0, Downloaded from https://onlinelibrary.wiley.com/doi/10.1002/solr.202500455 by Cagla Cetinkaya - Istanbul University , Wiley Online Library on [02/09/2025]. See the Terms and Conditions (https://onlinelibrary.wiley.com/terms-and-conditions) on Wiley Online Library for rules of use; OA articles are governed by the applicable Creative Commons License

architectures that maximize both the optical and electrical efficiency of CdTe-based devices, even with the thinnest possible active layer thicknesses. To achieve this goal, a DQL algorithm was developed to automatically optimize the thickness of each layer in the device architecture according to predefined photovoltaic performance targets. The proposed optimization process is based on the rigorous analysis of optical parameters and the parallel evaluation of photovoltaic performance using key indicators such as photon current density (J_{ph}). This integrated approach effectively addresses the complexities of ultra-thin multilayer CdTe solar cell designs in a disciplined manner, making a significant contribution to the development of high-efficiency, thin optoelectronic devices.

J_{ph} calculations are used to determine the photovoltaic performance of ultra-thin CdTe-based solar cells. These calculations are performed by analyzing the device's absorption spectrum in conjunction with the wavelength-dependent spectral irradiance of the AM1.5G solar spectrum. When these two key factors are considered, the wavelength-dependent variation of the J_{ph} parameter can be determined with high accuracy and used effectively for device performance optimization [18]. Detailed analyses of J_{ph} calculations have been extensively presented in our previous studies [47, 49, 59, 60]. In optical simulations, J_{ph} emerges as a relative performance indicator and is therefore employed as a critical optimization criterion [50, 59, 60].

Moreover, the optimization of optical and photovoltaic parameters of ultra-thin CdTe solar cells is carried out via the DQL algorithm, with careful consideration of the target optical and electrical performance metrics, particularly in cases involving broad-spectrum analyses. In this context, the wavelength-dependent refractive indices of each layer's material $\boldsymbol{n}(\lambda) = [n_1(\lambda), n_2(\lambda), \ldots, n_N(\lambda)]$, the extinction coefficients $\boldsymbol{k}(\lambda) = [k_1(\lambda), k_2(\lambda), \ldots, k_N(\lambda)]$, and the layer thicknesses $\boldsymbol{d} = [d_1, d_2, \ldots, d_N]$ are considered as the primary parameters. Additionally, a detailed analysis of the optical and photovoltaic spectra is required for designing multilayer solar cell structures, playing a crucial role in this optimization process. An absolute error function was defined to minimize the discrepancy between optical and photovoltaic parameters, and the layer thicknesses were optimized accordingly. Within a robust RL framework, optical and photovoltaic performance data derived from TMM calculations were used to guide the agent in exploring the optimal architecture. The optimization process in this study was modeled using an MDP, wherein TMM-based optical parameters (n, k, d) and target performance metrics (J_{ph}, transmittance, reflectance, absorption) were analyzed during environment simulations. Through iterative updates at each step, DQL continuously refines the parameters to learn the optimal structural configuration and design multilayer architectures that achieve high optical and photovoltaic performance. The theoretical foundation and computational methodology of this approach have been detailed in our previous studies [17, 18]. The neural network architecture and algorithmic flow of the developed model are illustrated in Figure 1c, with continuous refinement achieved using data from the simulation environment.

Full-stack optimization involves navigating a vast, discrete design space. Brute-force search would require billions of simulations when all layer thickness permutations are considered. The DQL algorithm circumvents this by focusing only on promising regions of the search space, guided by reward signals. This enables rapid convergence to high-efficiency configurations while minimizing computational effort, effectively resolving trade-offs such as those between absorber thickness and performance.

2.3.1 | Environment Space

In the developed DQL algorithm, the environment is modeled using optical and photovoltaic parameters derived from TMM calculations. In this framework, the DQL algorithm utilizes TMM computations as its environment. This approach enables the accurate modeling of light interactions in multilayer thin-film structures such as solar cells, which is essential for optimizing their optical and photovoltaic performance. The TMM is a widely accepted numerical technique used to calculate the optical characteristics—such as reflectance, transmittance, and absorbance—of multilayer thin-film structures. In this method, each layer of the solar cell is modeled as a planar, homogeneous, and isotropic medium with a complex refractive index. TMM calculates the propagation of electromagnetic waves through the interfaces and interiors of these layers by solving the continuity conditions of the electric and magnetic fields. These fields are related across boundaries using transfer matrices, which allow for the cumulative computation of the optical response of the entire stack. Importantly, the method takes into account interference effects, phase shifts, and amplitude variations that occur as the wave traverses different media with varying optical thicknesses. For each wavelength of interest, TMM provides the position-dependent electric field intensity, which is crucial for determining the absorption profile across the active region of the device. The method is particularly effective for analyzing semitransparent structures such as dielectric/metal/dielectric electrodes and photonic crystals, where constructive and destructive interference must be accurately captured to optimize both light harvesting and visible transparency. Therefore, TMM enables a highly precise evaluation of design modifications, supporting the optical optimization process of ultra-thin photovoltaic devices [17, 18, 47–50, 59–61].

For the calculation of optical properties, the extinction coefficient, refractive index, and thickness of each layer were used as fundamental parameters. At each step, the DQL agent analyzes the data provided by the TMM and is guided toward the optimal solution via the reward function. In doing so, the agent learns the design of an ultra-thin CdTe solar cell that achieves high photon current density and meets the target performance criteria. DQL enables the development of high-performance architectures by simultaneously optimizing both optical and photovoltaic objectives, thereby balancing multiple design requirements. TMM models quantify absorption across each layer, enabling accurate calculation of J_{ph}. TMM thus reveals how efficiently light is harvested in the CdTe layer versus lost in adjacent layers, providing a predictive framework for optimizing optical performance before fabrication.

2.3.2 | State Space

In the solar cell design process utilizing the DQL algorithm, the critical states are defined as the layer thicknesses, refractive indices, and extinction coefficients (Figure 1c). These parameters serve as direct determinants of optical and photovoltaic performance in

2367198x, 0, Downloaded from https://onlinelibrary.wiley.com/doi/10.1002/solr.202500455 by Cagla Cetinkaya - Istanbul University , Wiley Online Library on [02/09/2025]. See the Terms and Conditions (https://onlinelibrary.wiley.com/terms-and-conditions) on Wiley Online Library for rules of use; OA articles are governed by the applicable Creative Commons License

multilayer solar cell structures, having fundamental effects on light management and charge carrier dynamics within the device. In particular, layer thicknesses provide crucial control over the absorption, reflection, and transmission of light within the material, thereby shaping the overall device performance. Similarly, the refractive indices and extinction coefficients of materials also affect optical transitions and absorption processes by directing the interaction of electromagnetic waves with the material.

The DQL algorithm systematically adjusts these parameters to explore the multidimensional design space, aiming to identify the optimal configuration that maximizes the optical and photovoltaic performance of the device. In the RL process, the states represent the current physical and structural characteristics of the environment, and the algorithm explores the design space by executing actions based on these states. Within this framework, the DQL agent explores different configurations in the simulation environment by systematically varying the layer thicknesses, refractive indices, and extinction coefficients to achieve the target optical and photovoltaic performance metrics. Throughout the reinforcement optimization process, the agent learns which action yields the highest reward for each state, ultimately converging on the optimal device design. This process enables the agent to discover solar cell architectures that meet or exceed predefined performance targets, thereby introducing a significant advancement in the design process. By simultaneously considering both optical and photovoltaic performance criteria, this method provides an efficient optimization strategy for complex device design.

The layer materials and physical parameters used in the model, along with the defined value ranges for each parameter, are presented in Table 2. This table also indicates that if the boundary limits of the state parameters are exceeded, the model receives a negative reward, which subsequently triggers a new optimization iteration. This reward mechanism enhances the learning capacity of the algorithm, contributing to the maximization of the solar cell's performance.

2.3.3 | Action

The defined actions represent the process of adjusting the thicknesses of the solar cell layers that are to be optimized by the DQL algorithm. These actions form the basis of the artificial agent's decision-making mechanism and are designed to bring the optical and photovoltaic performance of the solar cell closer to the target values. The analyzed solar cell architecture consists of a five-layer structure, with the thickness of each layer controllable to at least 1 nm precision. The thickness of each layer can be increased or decreased by either 1 or 4 nm. As a result, each layer offers four distinct action choices, yielding a total of 20 unique action combinations across all layers. Each action corresponds to an increase or decrease in the thickness of a specific layer, and the agent uses these actions to determine the optimization direction at each step. This approach enables higher-resolution exploration of the parameter space in multilayer device architectures. However, the expansion of the action space also increases the algorithm's learning demands and the overall complexity of the optimization process. In this context, the DQL algorithm demonstrates its capability to discover optimal device architectures even within large and high-dimensional action spaces, thus standing out as a powerful optimization tool for optoelectronic device design.

TABLE 2 | Layer materials and physical parameters are used as states in the DQL algorithm, along with the defined value ranges for each parameter.

	Material	States	Range (nm)
Top opaque contact	Au	d_5	$5 \leq d_5 \leq 40$
Hole transport layer	MoO_3	d_4	$5 \leq d_4 \leq 70$
Active layer	CdTe	d_3	$100 \leq d_3 \leq 400$
Window layer	CdS	d_2	$30 \leq d_2 \leq 40$
Electron transport layer	SnO_2	d_1	$5 \leq d_1 \leq 70$
Transparent bottom contact	FTO	—	150

2.3.4 | Reward System

Within the RL framework, the reward function serves as the fundamental feedback mechanism that guides the agent's learning process and evaluates its performance. This reward, which represents the gain or loss associated with each action as it transitions the agent from the current state to a new one, is a critical parameter in the development of the agent's policy. The inherent inverse relationship between active layer thickness and J_{ph} makes optimization particularly complex in solar cell structures, where photon harvesting and energy conversion processes are involved. In this study, an innovative reward system was designed in accordance with the principles of multiobjective RL, effectively balancing the conflicting objectives of minimizing active layer thickness while maximizing J_{ph}. This system, integrated into the DQL algorithm, provides a multilayer reward architecture that enables simultaneous consideration of both optical and photovoltaic performance objectives.

In the developed reward function, an increase in the J_{ph} value obtained from the simulation environment (TMM calculations) following each action performed by the agent is supported by a positive reward of +20 points, while a constant or decreasing J_{ph} value results in a negative reward of −20 points. Additionally, an extra bonus reward of +10 points is assigned for performance outcomes that surpass the current highest J_{ph} value. This reward structure enables the agent to balance both optical and photovoltaic performance criteria within the Markov decision process framework of the simulation environment.

2.3.5 | Exploration and Exploitation

In the DQL algorithm, exploration and exploitation represent the agent's basic strategies for learning the environment and optimizing the design. At the beginning of the training process, the Q-network is initialized with random weights, resulting in random predictions of action values. During this early stage, the agent performs random actions to explore state-action pairs and gather information about the environment, a process referred to as exploration. As training progresses and Q-values begin to converge, the model produces more consistent action value estimates, and exploitation becomes dominant; i.e., the

2367198x, 0, Downloaded from https://onlinelibrary.wiley.com/doi/10.1002/solr.202500455 by Cagla Cetinkaya - Istanbul University , Wiley Online Library on [02/09/2025]. See the Terms and Conditions (https://onlinelibrary.wiley.com/terms-and-conditions) on Wiley Online Library for rules of use; OA articles are governed by the applicable Creative Commons License

agent selects the action with the highest estimated Q-value based on its current knowledge. However, at this point, the model risks becoming trapped in a local optimum, as limited exploration may reduce long-term performance. To mitigate this risk, the ∈-greedy strategy is employed. In this method, the agent continues to explore by selecting random actions with a probability of ∈, and exploits its current knowledge by choosing the optimal action with a probability of 1−∈. This balances exploration and exploitation, making the learning process more stable and effective. During training, the value of ∈ is gradually decreased (∈-decay strategy), allowing the model to prioritize exploration in the early stages and focus more on exploiting the learned knowledge in later stages. This balance enhances the agent's ability to acquire environmental information and optimize overall performance, resulting in a more robust learning process.

2.3.6 | Deep Q-Learning Algorithm

Through the holistic integration of the methods described above, the design of ultra-thin CdTe-based solar cells can be systematically optimized to meet the desired optical and photovoltaic performance criteria. The mathematical foundations and implementation details of the Q-network algorithms employed in this process have been comprehensively presented in our previous studies [17, 18].

The optimization problem between the active CdTe layer thickness and photon harvesting analyzed in this study poses specific challenges for conventional optimization methods due to its discrete and high-dimensional parameter spaces. For instance, genetic algorithms operating over large populations significantly increase the computational load, while Bayesian optimization often fails to deliver the desired performance in scenarios dominated by discrete parameters. Additionally, gradient-based methods, which rely on continuous and differentiable functions, are not directly applicable to this particular problem [62, 63]. In contrast, the DQL algorithm stands out due to its inherent compatibility with discrete action spaces and its ability to efficiently optimize high-dimensional state spaces through exploration and reward mechanisms within the RL framework. DQL has demonstrated effective performance, especially in optimization tasks aimed at maximizing critical photovoltaic parameters, such as photon current density (J_{ph}), while maintaining a minimal active layer thickness. In this context, the proposed DQL-based approach offers significant advantages over traditional optimization techniques in terms of both computational efficiency and the ability to achieve targeted performance metrics [64, 65].

In the context of this study, the addressed optoelectronic optimization problem involves a discrete, high-dimensional parameter space with competing objectives, such as maximizing J_{ph} while preserving acceptable minimum transparency. Traditional optimization methods often encounter inherent limitations in such complex design environments. For instance, genetic algorithms operate through large populations of candidate solutions per generation, which substantially increases computational load due to the high cost of repeated TMM and SCAPS-1D simulations. Particle Swarm Optimization (PSO), although effective in low-dimensional spaces, tends to converge prematurely and struggles with discrete design variables, reducing its applicability in this setting. Similarly, Bayesian optimization, which depends on surrogate modeling and probabilistic sampling, is typically better suited to continuous domains and loses efficiency in discrete and combinatorial search spaces. Gradient-based techniques, which require differentiable objective functions, are likewise incompatible with noncontinuous parameter landscapes. In contrast, the DQL algorithm is well-suited for discrete action spaces and leverages RL strategies to efficiently explore large state-action domains. Additionally, DQL demonstrates strong performance in multiobjective scenarios by dynamically balancing trade-offs between optical and electrical metrics. Accordingly, the proposed DQL-based framework offers a compelling alternative to conventional methods, providing both superior computational efficiency and high optimization quality in the design of ultra-thin photovoltaic structures [64–66].

3 | Result and Discussion

A novel approach that integrates deep learning and Q-learning methods has been proposed for the design of ultra-thin CdTe-based solar cells. The primary objective of this study is to identify solar cell architectures with maximum J_{ph} by optimizing all layers of an FTO/SnO_2/CdS/CdTe/MoO_3/Au structure using a DQL algorithm, particularly for devices incorporating ultra-thin CdTe active layers. In the literature, the optimal thickness of CdTe-based solar cells is generally reported to lie within the range of 1–2 micrometers [25]. This range enables high photovoltaic performance by ensuring strong photon absorption, efficient photon harvesting, and elevated quantum efficiency. However, in recent years, architectures featuring ultra-thin CdTe active layers (ranging from 100 nm to a few hundred nanometers) have demonstrated significant potential, especially in the development of lightweight, flexible, and low-material-consumption photovoltaic technologies [1, 25]. While ultra-thin CdTe structures pose certain challenges in terms of photon absorption, they offer notable advantages such as shorter carrier collection paths, reduced material usage, and enhanced environmental sustainability. In this context, understanding and optimizing the physical characteristics of ultra-thin CdTe architectures represents a crucial step toward advancing next-generation photovoltaic technologies.

In the literature, studies on solar cells with CdTe active layer thicknesses below 250 nm remain quite limited. The primary reason for this is the complexity of controlling grain size and grain boundaries during the fabrication of such thin active layers, which involve intricate morphological processes. However, with careful optimization of the magnetron sputtering technique, the possibility of producing ultra-thin CdTe layers in the 0.25–0.5 μm range has been demonstrated, enabling control over grain size and boundaries [25, 33]. Some studies have also suggested that ultra-thin CdTe layers of this scale may reduce the distance between the active layer and the back contact, potentially compromising long-term device stability. To address these technical uncertainties, Paudel et al. [35] conducted a comprehensive investigation using accelerated lifetime testing on devices with CdTe active layers ranging from 0.7 to 2.1 μm. These devices maintained their key performance parameters after 1000 h of light exposure and exhibited no significant degradation. These findings indicate that reducing the thickness of the active layer does not critically compromise device stability. Building upon

2367198x, 0, Downloaded from https://onlinelibrary.wiley.com/doi/10.1002/solr.202500455 by Cagla Cetinkaya - Istanbul University , Wiley Online Library on [02/09/2025]. See the Terms and Conditions (https://onlinelibrary.wiley.com/terms-and-conditions) on Wiley Online Library for rules of use; OA articles are governed by the applicable Creative Commons License

these studies, we have presented an effective design of solar cell architectures featuring ultra-thin CdTe active layers in the 100–400 nm range, motivated by the potential feasibility of fabricating such structures.

This study emphasizes the importance of conducting optical and electrical analyses and computations not only on the ultra-thin active layer but across all constituent layers of the device in solar cells; it is necessary to integrate and optimize the optical and electrical properties of all layers, including the window layer, ETL, HTL, buffer, and top contact, as well as the active layer that provides absorption. Optical transitions between layers, internal reflections, absorption characteristics, and the distribution of the electromagnetic field within the cell all directly affect photon harvesting. Meanwhile, carrier collection efficiency and interfacial transport significantly influence the electrical performance of the device. Therefore, optical parameters, including wavelength-dependent refractive indices, extinction coefficients, and layer thicknesses for all layers, as well as electrical properties, were evaluated using a holistic approach. In this context, the DQL algorithm was employed to explore optimal structural designs over a broad parameter space, and the resulting configurations were evaluated based on optical spectrum analyses and photovoltaic performance metrics (J_{ph}). Through these analyses, this study contributes to the development of highly efficient and sustainable solar cells by enabling the simultaneous optimization of both optical and electrical performance in ultra-thin CdTe-based architectures.

In this section, the optical and photovoltaic performances of solar cell designs optimized using the DQL algorithm featuring ultra-thin CdTe absorber layers with thicknesses of 100, 150, 200, and 400 nm are discussed in detail. This study emphasizes the importance of integrating both optical and electrical optimization in future ultra-thin CdTe solar cell designs, providing a significant roadmap toward achieving high-efficiency targets.

3.1 | Design of Ultra-Thin CdTe-Based Solar Cells with Maximum Photon Harvesting

Reducing the thickness of the active layer in ultra-thin CdTe-based solar cells leads to significant losses that limit the potential for improving photovoltaic performance. In the FTO/SnO_2/CdS/CdTe/MoO_3/Au architecture considered in this study, effective photon harvesting was optimized by accounting for the wavelength-dependent behavior of the refractive index and extinction coefficient across all layers. In particular, the Au top contact layer, which exhibits high reflectivity in the visible spectrum and thickness-dependent electrical conductivity, emerged as a critical factor in balancing electromagnetic wave propagation and overall device performance.

In this study, designs that maximize photon harvesting were targeted for solar cells with ultra-thin CdTe active layers, using the DQL algorithm at thicknesses of 100, 150, 200, and 400 nm. There exists an inverse relationship between ultra-thin active layer thickness and J_{ph}, and the simultaneous optimization of these parameters presents a highly complex design challenge. In this context, the DQL-based optimization strategy developed in this work provided an effective solution framework for this multidimensional and multiobjective problem, serving as a powerful tool to enhance J_{ph} performance and optimize photon harvesting. As previously detailed, the reward function used in the study was designed and optimized to account for both optical and photovoltaic performance metrics. The DQL algorithm was trained over a total of 1500 episodes, and its performance was evaluated based on training loss and total reward metrics.

Figure 2a,b present the loss and normalized total reward variations, respectively, observed during the training process of the DQL algorithm for four different ultra-thin CdTe-based solar cell structures (SC-100, SC-150, SC-200, SC-400). These figures provide critical data for evaluating both the effectiveness of the optimization process and the learning dynamics. The findings clearly demonstrate the effectiveness of DQL in achieving the targeted optimization criteria throughout the training period.

Loss values are quite high during the initial stages of the DQL algorithm (approximately 4.5×10^7), but they decrease steadily as the training process progresses. In particular, a rapid decrease was observed in the first 250 episodes, indicating that the algorithm converges to optimal parameter sets by cyclically reducing errors. Among the analyzed structures, the SC-400 shows a higher initial loss compared to the others, suggesting that the optimization space for the 400 nm-thick active layer may be more complex and extensive. However, as training progresses, the loss values for all structures approach near-zero levels, confirming that the DQL algorithm successfully discovers optimal parameter configurations for each design. This downward trend demonstrates the algorithm's ability to effectively resolve the complex interactions between layer thickness and optical-electrical parameters and to identify structures that maximize device performance. These results indicate that the learning process concluded stably and that the algorithm achieved a robust optimization routine by minimizing errors. Notably, after the 250th episode, all episodes yielded optimized configurations for the targeted ultra-thin CdTe-based solar cell architectures.

The normalized total reward values represent the normalized form of rewards obtained by the algorithm throughout the training process. These values reflect the algorithm's capacity and stability in achieving optimal performance. In the initial phase (approximately the first 250 episodes), the total reward values for all structures remain relatively low and exhibit fluctuations, indicating that the algorithm is in the exploration phase, testing various parameter combinations. As the training progresses (between episodes 250 and 750), the SC-400 obtains higher reward values compared to the other configurations, showing a more rapid adaptation to the optimization process, with its reward curve rising noticeably. This behavior suggests that, due to the broader optical absorption region associated with a 400 nm-thick active layer, the J_{ph} parameter can be optimized more stably. Meanwhile, the reward curves for the SC-100 and SC-150 also increase over time, indicating that the algorithm effectively discovers parameter sets that provide optimal photon harvesting in thinner active layers. After approximately the 400th episode, fluctuations in the reward curves diminish, and the curves approach a stable plateau level. This indicates a transition from the exploration phase to the exploitation phase, during which the algorithm consolidates the optimal parameter sets. In other words, the solar cells with CdTe active layer thicknesses

2367198x, 0, Downloaded from https://onlinelibrary.wiley.com/doi/10.1002/solr.202500455 by Cagla Cetinkaya - Istanbul University , Wiley Online Library on [02/09/2025]. See the Terms and Conditions (https://onlinelibrary.wiley.com/terms-and-conditions) on Wiley Online Library for rules of use; OA articles are governed by the applicable Creative Commons License

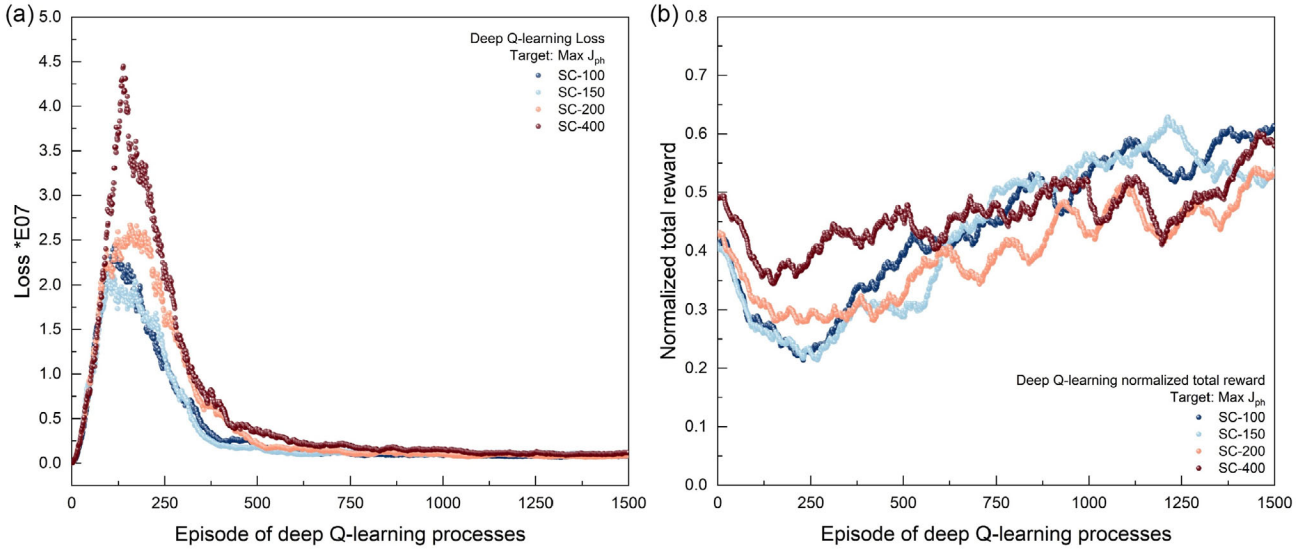


FIGURE 2 | Episode-based variations of (a) Loss and (b) Normalized total reward values for ultra-thin CdTe active layer-based solar cells (SC-100, SC-150, SC-200, SC-400) optimized using the DQL algorithm.

proposed by the DQL algorithm at this stage are considered optimal structures capable of achieving maximum J_{ph} performance.

These results confirm that the optimization process for solar cells with ultra-thin CdTe active layers was completed and that the DQL algorithm is capable of holistically optimizing both optical and electrical parameters. For each of the solar cells with thicknesses of 100, 150, 200, and 400 nm, the stabilization of both the loss and reward curves into well-defined plateaus demonstrates that theoretical challenges and engineering constraints were effectively overcome. This outcome verifies the potential of the algorithm to be used efficiently in achieving the desired optimal performance.

The DQL algorithm's ability to discover optimal layer thickness combinations across different episodes and steps significantly enhances the photovoltaic performance of ultra-thin CdTe-based solar cell designs. In the FTO/SnO_2/CdS/CdTe/MoO_3/Au structure, the optimum thickness values identified by the algorithm for all layers except FTO played a critical role in determining the most efficient configurations yielding maximum J_{ph} values. Details of selected top-performing structures proposed by the DQL algorithm at various episodes and steps are presented in Table 3. This table highlights both the algorithm's exploratory capability within the design space and the substantial influence of layer thickness parameters on device performance in ultra-thin CdTe-based solar cells, thereby making a significant contribution to the optimization process of the study.

Table 3 highlights the DQL algorithm's ability to discover optimal parameter sets during different episodes and steps in the design of ultra-thin CdTe solar cells, particularly the contribution of upper-layer thickness optimization to device performance. SC-100 provided relatively lower J_{ph} values, while SC-400 demonstrated maximum J_{ph} performance. The episodes at which maximum J_{ph} was obtained for each solar cell design were determined as 606 (SC-100), 444 (SC-150), 527 (SC-200), and 770 (SC-400), respectively. Figure 3a–f is presented to detail how J_{ph} was maximized throughout the steps in these episodes proposed by the DQL algorithm and how each independent variable, namely layer thicknesses (SnO_2, CdS, CdTe, MoO_3, and Au), was optimized and evolved on a step-by-step basis. In Figure 3, the algorithm's exploration and exploitation behaviors across the design space are clearly observable, providing insight into which layer thickness modifications played a critical role in achieving the maximum J_{ph}. Figure 3a illustrates the stepwise variation of the maximum J_{ph} value, while Figures 3b–f show the step-by-step evolutionary behavior of the optimized thicknesses for the ETL, window layer, absorber layer, HTL, and top metal contact, respectively. These results are crucial for understanding how the DQL algorithm manages the independent variables within each solar cell design's state space and how it navigates toward optimal solutions at different step levels.

The theoretical J_{sc} limit for CdTe-based solar cells, as defined by the Shockley–Queisser model, is approximately 31 mA/cm^2. In contrast, the J_{ph} values obtained in this study exceed this threshold because their computation is based solely on optical absorption, under the idealized assumption that every absorbed photon generates an electron–hole pair contributing fully to the photocurrent. As such, J_{ph} serves as a relative indicator of the maximum achievable photocurrent in the absence of recombination and electrical losses. Upon reviewing the J_{ph} values presented in Table 3, it becomes evident that these idealized current densities surpass the Shockley–Queisser limit for J_{sc}. This is an expected outcome, as J_{ph} estimations deliberately neglect nonradiative recombination and carrier transport inefficiencies to facilitate the comparative assessment of device architectures based on their optical response. For reference, CdTe-based devices operating at the Shockley–Queisser limit typically exhibit photovoltaic parameters such as V_{oc} around 1.2 V, J_{sc} near 31 mA/cm^2, and FF of ~ 90%. While J_{ph} does not represent the actual operating current, it is widely utilized in the literature to guide structural optimization based on photon absorption potential [51].

In the DQL-optimized ultra-thin CdTe-based solar cell (FTO/SnO_2/CdS/CdTe/MoO_3/Au), considering that light enters the cell through the FTO and subsequently the SnO_2 layers, it becomes

2367198x, 0, Downloaded from https://onlinelibrary.wiley.com/doi/10.1002/solr.202500455 by Cagla Cetinkaya - Istanbul University , Wiley Online Library on [02/09/2025]. See the Terms and Conditions (https://onlinelibrary.wiley.com/terms-and-conditions) on Wiley Online Library for rules of use; OA articles are governed by the applicable Creative Commons License

TABLE 3 | Selected designs achieving maximum photocurrent density for ultra-thin CdTe-based solar cells optimized by the Deep Q-Learning algorithm.

Targetultra-thin active layer	States – material thickness [d_{SnO2},d_{CdS},d_{CdTe},d_{MoO3},d_{Au}] (nm)	Episode	Step	J_{ph} (mA cm^{-2})
100 nm CdTeSC-100	[70, 40, 100, 26, 40]	606	180	42.868
	[70, 40, 100, 27, 40]	722	248	42.862
	[70, 40, 100, 28, 40]	626	235	42.851
150 nm CdTeSC-150	[70, 40, 150, 5, 40]	444	218	46.584
	[70, 40, 150, 5, 40]	540	201	46.584
	[70, 40, 150, 5, 40]	680	245	46.584
200 nm CdTeSC-200	[70, 40, 200, 5, 40]	527	211	47.235
	[70, 40, 200, 7, 40]	738	246	47.226
	[70, 40, 200, 8, 40]	602	179	47.221
400 nm CdTeSC-400	[70, 40, 400, 30, 40]	770	250	51.946
	[70, 40, 400, 22, 40]	732	92	51.941
	[70, 40, 400, 30, 40]	740	226	51.941

evident that layer thicknesses play a critical role in both photon harvesting and carrier collection efficiency. As shown in Figure 3a, the SC-400 (with a 400 nm active layer) exhibits the highest J_{ph} performance (~52 mA/cm^2), whereas the SC-100 achieves a lower J_{ph} (~42.8 mA/cm^2). This result confirms that increasing the thickness of the active layer enhances photon harvesting, thereby optimizing J_{ph}. In Figure 3b, which illustrates the stepwise evolution of SnO_2 layer thickness, the algorithm optimizes this parameter to 70 nm across all ultra-thin CdTe-based solar cells. This thickness enables both low optical reflection and effective carrier collection. This thickness reduces the initial absorption losses of the incident light, acting as an efficient optical window in the ETL, thereby optimizing the transparency-conductivity balance of the device.

In Figure 3c, the CdS layer thickness is optimized. For all structures, the CdS thickness was optimized to 40 nm. This thickness prevents the absorption of short-wavelength photons within the CdS layer, facilitating their transmission to the p-type CdTe layer and thereby enhancing effective photon harvesting. Moreover, avoiding excessive thickness in this layer minimizes parasitic absorption and optical losses. Figure 3d presents the optimization process for the CdTe active layer thickness. In all structures, the thickness of the CdTe active layer was set as intended and adjusted to maximize optical absorption. Increasing the thickness, particularly in the red and near IR regions, enhances photon absorption and consequently improves J_{ph}. In the SC-100 and SC-150, lower J_{ph} was observed due to the thinner active layers. This can be attributed to the reduced number of absorbed photons resulting from the limited optical absorption depth.

In Figure 3e, the MoO_3 thickness was optimized in the range of 5–30 nm, with stabilization at approximately 30 nm, particularly in the SC-400. This thickness minimizes optical losses (e.g., reflection and absorption) while optimizing hole injection and supporting carrier collection efficiency at the interface region. These factors contributed to the stabilization of the J_{ph} value. Figure 3f illustrates the thickness optimization of the Au top metal contact. In all configurations, the Au layer was optimized to 40 nm. This thickness enhances internal reflection by leveraging the semireflective properties of the metal layer, thereby enabling increased photon absorption within the active layer. Additionally, the high conductivity of the Au layer reduces the series resistance of the top contact, further contributing to photovoltaic efficiency. Through this strategy, photons within the device are reflected back into the active layer, increasing the probability of absorption and maximizing photon harvesting.

To account for optical losses in the front layers, the parasitic absorption in the SnO_2 and CdS layers was carefully taken into consideration. These layers, while essential for charge transport and optical window functions, can absorb a portion of the incident light, particularly in the short-wavelength range ($\lambda < 500$ nm), thereby limiting photon availability at the CdTe absorber. Literature reports indicate that SnO_2 exhibits absorption coefficients up to 10^3–10^4 cm^{-1} in the near-UV region [67–69], while CdS layers thicker than 50 nm can cause up to 15% absorption loss in this spectral range [70]. In the present study, the DQL algorithm effectively mitigated these losses by optimizing the thicknesses of SnO_2 and CdS to 70 and 40 nm, respectively, which is consistent with the values reported for high-efficiency ultra-thin CdTe devices [48, 51]. Moreover, the optical back-reflection provided by the 40 nm Au top contact enhances internal light trapping and compensates for front-layer absorption by increasing the optical path length within the absorber. This integrated design approach strengthens overall photon harvesting and supports higher photovoltaic efficiency, particularly in ultra-thin device architectures.

The optical and electrical characteristics of SnO_2, CdS, and MoO_3 have a significant influence on the performance of ultra-thin CdTe solar cells. SnO_2 offers high transparency and electron transport, but can introduce losses in the UV range. CdS provides junction alignment while reducing transmittance if it is overly thick. MoO_3 enhances hole extraction due to favorable band alignment but requires careful thickness control to avoid optical

2367198x, 0, Downloaded from https://onlinelibrary.wiley.com/doi/10.1002/solr.202500455 by Cagla Cetinkaya - Istanbul University , Wiley Online Library on [02/09/2025]. See the Terms and Conditions (https://onlinelibrary.wiley.com/terms-and-conditions) on Wiley Online Library for rules of use; OA articles are governed by the applicable Creative Commons License

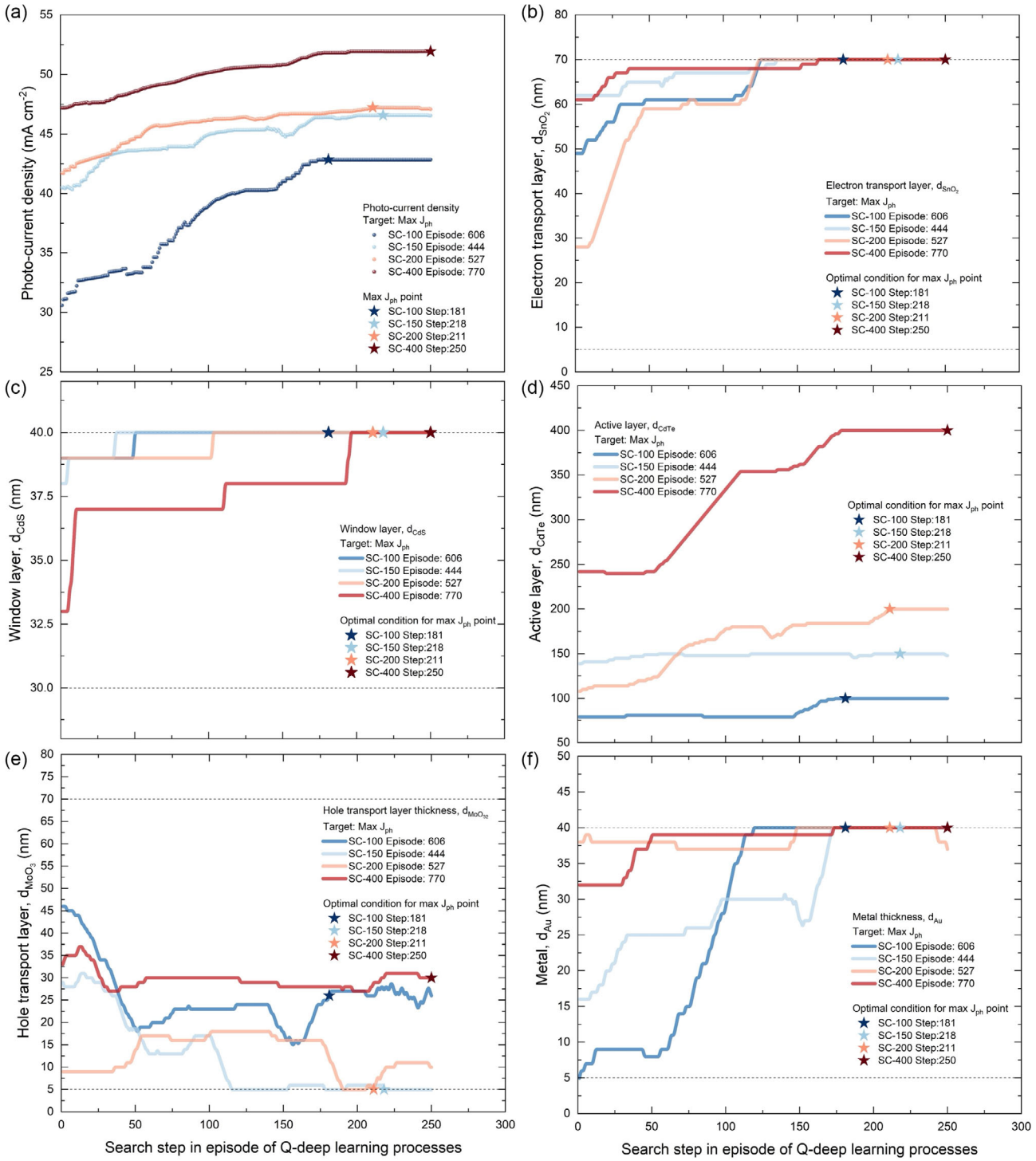


FIGURE 3 | Stepwise evolution of parameters leading to maximum J_{ph} performance in ultra-thin CdTe-based solar cells optimized by the DQL algorithm. Evolution of (a) maximum J_{ph} across steps, (b) ETL thickness, (c) window layer thickness, (d) active layer thickness, (e) HTL thickness, and (f) top metal contact thickness optimized at each step.

loss. Properly balancing these layers ensures minimal parasitic absorption and efficient carrier dynamics in sub-400 nm architectures.

These findings demonstrate that the DQL algorithm holistically optimizes both optical and electrical processes for each layer. Optimizing the transparency and refractive indices of the SnO_2 and CdS layers directly contributed to increasing J_{ph} values by enhancing the photon harvest of the active layer. Similarly, optimizing the thicknesses of the MoO_3 and Au layers significantly improved device performance by enhancing carrier injection efficiency and internal optical reflection. Collectively, these results clearly reveal that the comprehensive optimization of layer thicknesses in conjunction with optical and electrical parameters plays a critical role in achieving maximum photon harvesting and J_{ph} performance in ultra-thin CdTe-based solar cells.

2367198x, 0, Downloaded from https://onlinelibrary.wiley.com/doi/10.1002/solr.202500455 by Cagla Cetinkaya - Istanbul University , Wiley Online Library on [02/09/2025]. See the Terms and Conditions (https://onlinelibrary.wiley.com/terms-and-conditions) on Wiley Online Library for rules of use; OA articles are governed by the applicable Creative Commons License

3.2 | Optical and Photovoltaic Performance of the Ultra-Thin CdTe-Based Solar Cell Designed via Deep Q-Learning

In this section, the optical and photovoltaic performance of the ultra-thin CdTe-based solar cells optimized using the DQL algorithm in the previous section is examined in detail. For four different device configurations with active layer thicknesses of 100, 150, 200, and 400 nm, optimal parameter sets were determined and evaluated in terms of both optical and electrical performance. Optical characterizations were conducted using the TMM, and the light transmittance and absorption profiles of each structure, along with their photon harvesting potentials, were analyzed. This analysis revealed how ultra-thin active layers contribute to efficient photon absorption and how interlayer optical transitions affect overall device performance.

The band diagrams created for each structure enabled the analysis of device-internal physical processes, such as carrier collection, potential barriers, and interface transitions. The effect of optimization on photovoltaic performance was explained in detail. The ultra-thin CdTe-based structures optimized via the DQL algorithm were comprehensively evaluated through their band diagrams and J–V characteristics to assess the integration of optical absorption and photovoltaic performance. This demonstrated the suitability of the proposed structures for high-performance ultra-thin CdTe-based solar cells. Photovoltaic performance parameters were evaluated using SCAPS-1D simulations; critical metrics such as V_{oc}, J_{sc}, FF, and PCE were calculated and evaluated for each optimized structure.

Figure 4 presents the detailed optical spectra of the optimized ultra-thin CdTe-based solar cells with active layer thicknesses of 100, 150, 200, and 400 nm. These spectra are of critical importance for directly evaluating the optical characteristics of the cells and their photon-harvesting potential.

When examining the transmittance spectra of all optimized structures within the 300–1200 nm wavelength range, it is observed that transmittance remains low in the short-wavelength region (300–500 nm) and shows a slight increase in the longer-wavelength region (700–1200 nm). This behavior is attributed to the strong absorption or reflection characteristics of the SnO_2 and CdS layers, particularly at shorter wavelengths. In structures with a 100 nm-thick active layer, the transmittance curve is slightly higher than that of the others, indicating that the ultra-thin active layer permits partial light transmission, which may lead to relatively lower photon harvesting. In contrast, structures with a 400 nm-thick active layer exhibit reduced transmittance, suggesting enhanced optical absorption.

The absorption curves exhibit a clear upward trend with increasing active layer thickness. In particular, the structure with a 400 nm-thick active layer demonstrates the highest absorption capacity in the visible and near IR region (600–900 nm), indicating optimized photon harvesting. In contrast, structures with a 100 nm-thick active layer show limited absorption in terms of both intensity and spectral width, with increased optical losses observed at higher wavelengths. This outcome reveals that optical absorption is constrained in ultra-thin active layers, which negatively affects photovoltaic performance. This effect is directly reflected in the J_{ph} characteristics.

In the FTO/SnO_2/CdS/CdTe/MoO_3/Au structure, light first enters through the SnO_2 layer. The SnO_2 and CdS layers function as optical windows, enabling short-wavelength photons to reach the p-type CdTe active layer. However, the thickness optimization of these layers played a critical role in minimizing reflection losses at the front interface and thereby supported enhanced photon harvesting. In structures with a 400 nm-thick active layer, the p-CdTe layer effectively absorbed incident photons, leading to maximized J_{ph} values. The optimized thicknesses of the MoO_3 and Au back contact layers (with Au set at 40 nm in all structures) created internal reflection at the rear interface, redirecting

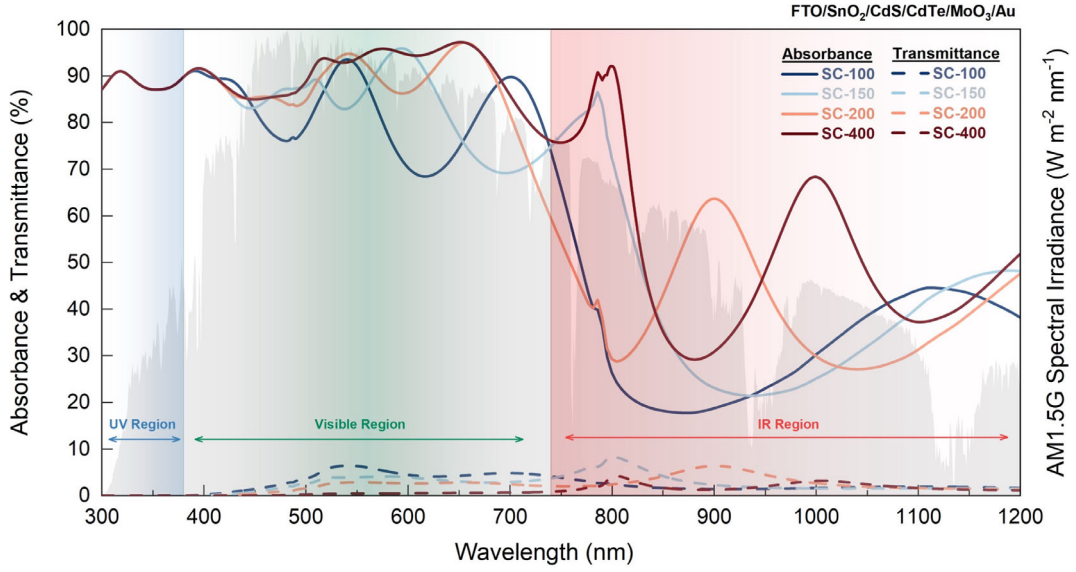


FIGURE 4 | Transmittance and absorption spectra of optimized ultra-thin CdTe-based solar cells. The spectral behavior of different active layer thicknesses is presented to comparatively reveal photon harvesting and optical transmittance as a function of wavelength. The gray background curve represents the AM 1.5G spectral irradiance.

2367198x, 0, Downloaded from https://onlinelibrary.wiley.com/doi/10.1002/solr.202500455 by Cagla Cetinkaya - Istanbul University , Wiley Online Library on [02/09/2025]. See the Terms and Conditions (https://onlinelibrary.wiley.com/terms-and-conditions) on Wiley Online Library for rules of use; OA articles are governed by the applicable Creative Commons License

unabsorbed light back into the active layer and extending the optical path length. This optical back-reflection effect directly contributes to device performance by enhancing absorption efficiency, particularly at longer wavelengths. As a result, increased active layer thickness in the optimized ultra-thin CdTe solar cells broadened and intensified the absorption curves, enabling greater photon harvesting and, consequently, improved J_{ph} performance. Simultaneously, the optical reflectivity of the Au top layer enhanced internal reflection, reducing optical losses and rendering all structures opaque. These analyses demonstrate that the layer thickness parameters proposed by the DQL algorithm play an integrated and optimizing role in both optical and photovoltaic performance. Furthermore, the ultra-thin CdTe cells designed using DQL exhibited efficient absorption characteristics and photon harvesting within the wavelength regime governed by the AM1.5G solar spectrum.

The band diagrams of the ultra-thin CdTe-based solar cells, whose active layer thicknesses were optimized using the DQL algorithm, are presented in Figure 5. These diagrams were generated through SCAPS-1D simulations based on the numerical solution of the Poisson equation. The cells with the FTO/SnO_2/CdS/CdTe/MoO_3/Au architecture were analyzed under zero-bias conditions to investigate carrier collection, potential barriers, and interfacial transitions in detail. The band diagrams corresponding to each optimized active layer thickness (100, 150, 200, and 400 nm), along with the other optimized layers, visually depict the influence of electron and hole transport processes on device performance. These diagrams illustrate the potential distribution within the device and the position of the Fermi level, contributing to a deeper understanding of the physical foundations underlying photovoltaic performance. Each band diagram details the conduction band (E_c), valence band (E_v), and Fermi level (E_F) within the FTO/SnO_2/CdS/CdTe/MoO_3/Au architecture, elucidating how the optimized layer thicknesses affect potential barriers and carrier transport across the device.

The band profiles of the optimal ultra-thin CdTe-based structures clearly demonstrate how the layer thicknesses optimized via DQL affect the internal potential distribution, carrier transport, and overall photovoltaic performance. In all structures, distinct band offsets are observed at the SnO_2, CdS, CdTe, and MoO_3/Au interfaces for both the conduction and valence bands. These staggered alignments indicate that the optical window and carrier-selective contact layers have been optimized to achieve ideal band alignment. The energy barriers (ΔE_c and ΔE_v) formed at the SnO_2/CdS and CdS/CdTe interfaces facilitate efficient electron and hole transport, while the depth and width of the potential wells have been optimized to minimize recombination losses of photogenerated carriers.

As the thickness of the active layer increases (from 100 to 400 nm), no significant changes are observed in the potential gradients within the CdTe layer. This indicates that tunneling effects are not dominant in the optimized designs and that bulk transport mechanisms prevail. Furthermore, the increase in active layer thickness enhances photon absorption, thereby improving the generation profile and potentially enabling higher quantum efficiency within the potential distribution. In the structure with a 400 nm active layer, no distinct potential barrier is observed within the CdTe layer, and carrier transport appears to be uniformly distributed, suggesting that diffusion-based carrier collection is the dominant mechanism. The optimized thicknesses in all structures enable the upward stepwise alignment of the conduction band in the SnO_2 and CdS layers, as well as the formation of hole-blocking barriers in the valence band. This band alignment promotes selective transport of electrons toward the SnO_2 layer and holes toward the MoO_3/Au contacts, contributing to a high FF and open-circuit voltage. No sharp potential barriers are observed at the MoO_3/Au interface in the conduction band, indicating a low-resistance contact that facilitates hole injection without requiring tunneling mechanisms. Across all band diagrams, no abrupt or steep potential spikes or band overlaps are present, further confirming that tunneling effects are not dominant. Thus, carrier transport occurs through diffusion and drift mechanisms. The band alignment at the SnO_2/CdS and CdTe/MoO_3 interfaces effectively limits recombination losses and enhances carrier collection efficiency.

Ultimately, the optimized ultra-thin CdTe-based structures, with their refined layer thickness parameters, exhibit ideal potential profiles for carrier collection, recombination suppression, and selective transport in both optical and electrical processes. In each structure, band alignments have been ideally achieved, and the potential barriers have been deliberately tuned to support optimal performance. As a result, tunneling effects are effectively suppressed, the bulk-diffusion-based carrier collection mechanism is reinforced, and an ideal potential distribution is attained for efficient device operation. The optimization of these structures once again demonstrates the DQL algorithm's ability to integrate and manage optical and electrical parameters in a unified manner.

SCAPS-1D solves Poisson equations and continuity equations for electrons and holes, taking into account the doping profiles, material parameters (e.g., as given in Table 1; band gap, electron and hole mobilities, dielectric constant), and interface properties of optimal ultra-thin CdTe-based solar cells. This allows the derivation of the *J–V* characteristics by considering the diffusion and drift processes of photogenerated carriers resulting from light absorption. Accordingly, *J–V* curves were calculated for both dark and illuminated conditions using SCAPS-1D for each optimized structure, and the device's fundamental performance parameters, such as V_{oc}, J_{sc}, FF, and PCE, were obtained. Figure 6a presents the *J–V* characteristics of four different optimized ultra-thin CdTe-based solar cell structures with active layer thicknesses of 100, 150, 200, and 400 nm. Figure 6b illustrates the corresponding power–voltage (P–V) characteristics, visually highlighting the maximum power point behavior of each device. The obtained results are detailed in Table 4, which provides a comparative evaluation of the photovoltaic performance parameters of the optimized structures.

In this section, the photovoltaic performance of the structures proposed by the DQL algorithm is thoroughly analyzed using the *J–V* and P–V curves obtained via SCAPS-1D. The impact of the optimized layer thicknesses on device efficiency is comprehensively evaluated, providing detailed insights into how effectively the DQL-based optimization contributes to the overall device performance.

2367198x, 0, Downloaded from https://onlinelibrary.wiley.com/doi/10.1002/solr.202500455 by Cagla Cetinkaya - Istanbul University , Wiley Online Library on [02/09/2025]. See the Terms and Conditions (https://onlinelibrary.wiley.com/terms-and-conditions) on Wiley Online Library for rules of use; OA articles are governed by the applicable Creative Commons License

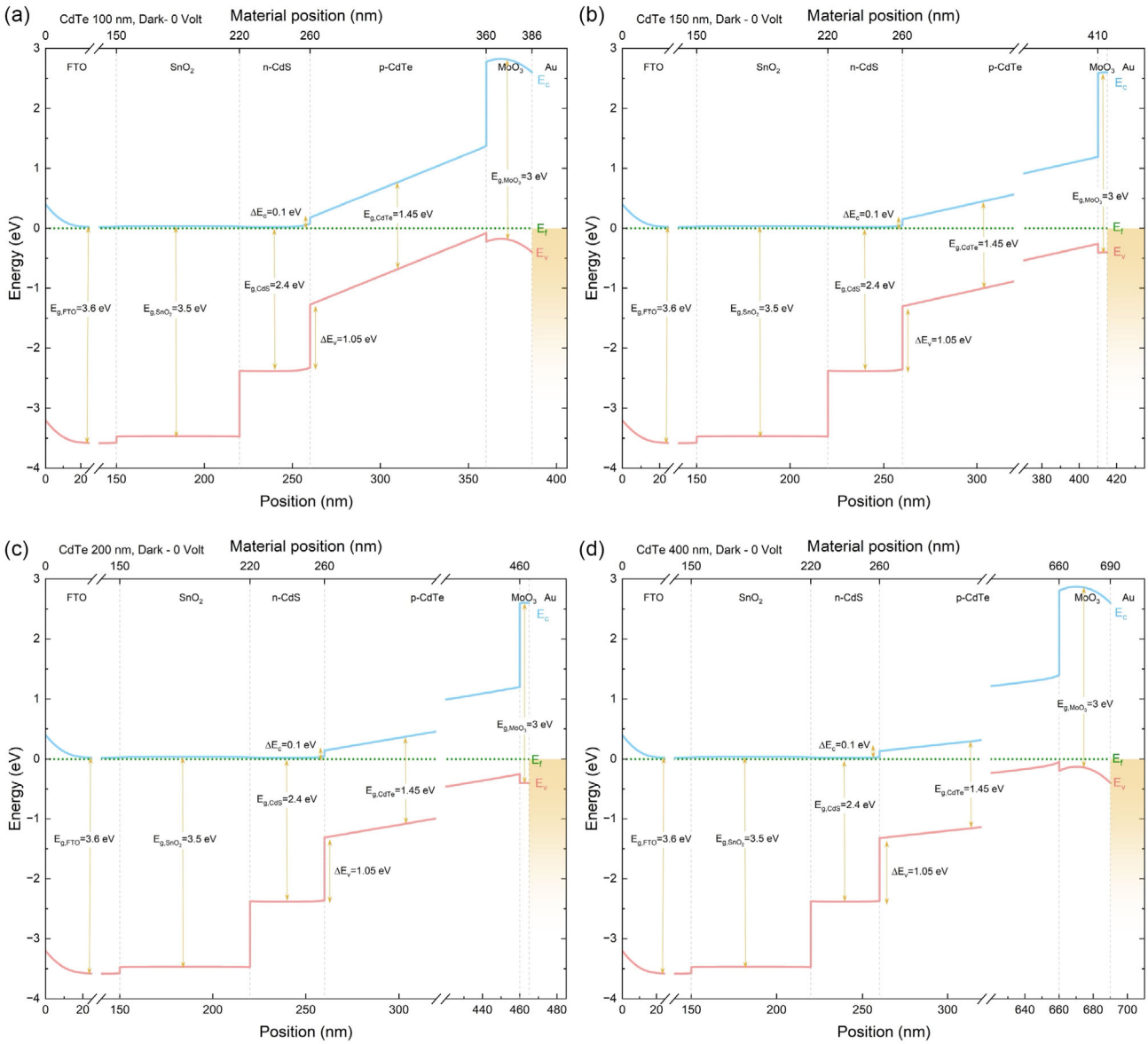


FIGURE 5 | Energy band diagrams of the optimal ultra-thin CdTe-based SC structures under 0 V bias. Band diagram of (a) SC-100 (Episode: 606), (b) SC-150 (Episode: 444), (c) SC-200 (Episode: 527), and (d) SC-400 (Episode: 770).

As shown in Table 4, the V_{oc} of all optimized structures remains within a narrow range of 0.927 to 0.977 V. This consistency indicates that, despite the variations in the optimized layer thicknesses, proper band alignment and stable potential barriers have been maintained across all devices. This finding is also clearly reflected in the previously analyzed band diagrams. At the SnO_2/CdS/CdTe and CdTe/MoO_3/Au interfaces, the potential profiles exhibit uniform band alignment regardless of changes in layer thickness, thereby confirming the establishment of selective carrier transport. Moreover, this band alignment effectively minimizes recombination losses, contributing to the maintenance of a high V_{oc}.

As the active layer thickness increased (from 100 to 400 nm), a significant increase in J_{sc} values was observed: from 11.83 to 20.86 mA/cm^2. This increase is directly correlated with the enhancement in optical absorption spectra. The absorption spectra obtained using TMM indicate that photon absorption in the visible and near IR regions increases significantly as the active layer thickness increases. In particular, the 400 nm thick active layer leads to increased optical absorption depth and a higher number of absorbed photons in the p-CdTe region, thereby enhancing photon harvesting and boosting the J_{sc}. In contrast, for structures with 100 nm active layers, the ultra-thin absorber limits optical absorption capacity, resulting in relatively lower J_{sc}s.

The PCE values exhibit a direct correlation with the J_{sc} parameter and increase with the thickness of the active layer. This trend confirms that increasing the active layer thickness enhances optical absorption, thereby strengthening photon harvesting and ultimately improving the device's overall PCE. Notably, FF has remained at 81% across all structures, indicating that the optimized layer thicknesses do not adversely affect the series and shunt resistances within the device and that charge transport mechanisms are effectively maintained.

2367198x, 0, Downloaded from https://onlinelibrary.wiley.com/doi/10.1002/solr.202500455 by Cagla Cetinkaya - Istanbul University , Wiley Online Library on [02/09/2025]. See the Terms and Conditions (https://onlinelibrary.wiley.com/terms-and-conditions) on Wiley Online Library for rules of use; OA articles are governed by the applicable Creative Commons License

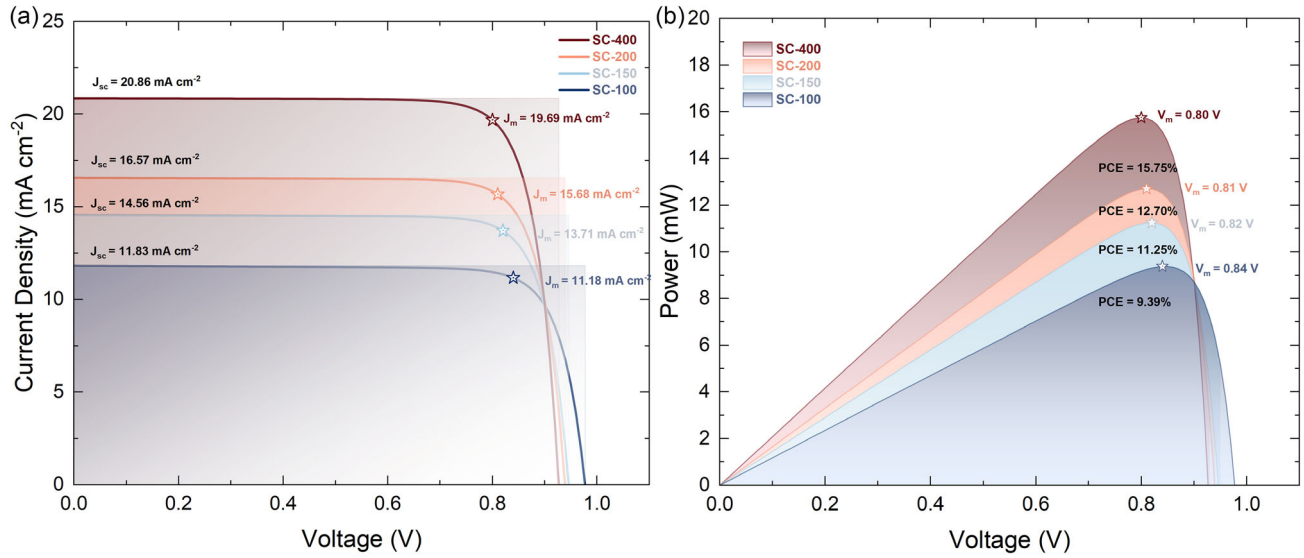


FIGURE 6 | (a) *J–V* and (b) P–V characteristics of the optimal ultra-thin CdTe-based solar cells calculated using SCAPS-1D.

TABLE 4 | Photovoltaic performance parameters of the optimal ultra-thin CdTe-based solar cells.

Targetultra-thin active layer	States – material thickness [d_{SnO2},d_{CdS},d_{CdTe},d_{MoO3},d_{Au}] (nm)					J_{ph} (mA/cm^2)	V_{oc} (V)	J_{sc} (mA/cm^2)	FF (%)	PCE (%)
	SnO_2	CdS	CdTe	MoO_3	Au					
100 nm CdTeSC-100	70	40	100	26	40	42.86	0.977	11.83	81.18	9.39
150 nm CdTeSC-150	70	40	150	5	40	46.58	0.946	14.56	81.62	11.25
200 nm CdTeSC-200	70	40	200	5	40	47.24	0.939	16.57	81.65	12.70
400 nm CdTeSC-400	70	40	400	30	40	51.94	0.927	20.86	81.43	15.75

Notably, even the SC-100, featuring an ultra-thin active layer thickness of 100 nm, achieved a PCE of 9.39% due to the optimized layer thicknesses. This is particularly remarkable given the limited photon absorption depth typically associated with ultra-thin active layers. Through the application of the DQL algorithm, optical losses were minimized, and photon harvesting was maximized by optimizing the thicknesses of the optical window layers (SnO_2 and CdS), the active layer (CdTe), and the carrier-selective contact layers (MoO_3/Au). Similarly, the SC-150 (with a 150 nm active layer) demonstrated a notable efficiency of 11.25% in terms of optical performance. These results clearly demonstrate that high-efficiency operation in ultra-thin solar cells can be achieved through the integrated optical and electrical optimization of all device layers rather than relying solely on active layer thickness. The DQL algorithm successfully identified thicknesses that minimize reflection and absorption in the SnO_2 and CdS layers while simultaneously optimizing optical internal reflection and carrier injection in the MoO_3 and Au layers. This holistic optimization significantly enhanced both photon harvesting and carrier collection processes within the device. Thanks to this comprehensive optimization, ultra-thin CdTe solar cells can achieve high photon harvesting and, consequently, high PCEs despite their thinned active layers, supporting both optical and electrical processes.

Unlike conventional approaches that primarily focus on tuning the CdTe absorber thickness while keeping other layers fixed, the present study employs a full-stack optimization framework in which all five key layers—SnO_2, CdS, CdTe, MoO_3, and Au—are simultaneously optimized using DQL. This integrated approach enabled the identification of ultra-thin CdTe-based architectures with high photovoltaic performance, even at absorber thicknesses as low as 100 nm. As illustrated in [33], prior studies reported that devices with 250–500 nm CdTe absorbers typically achieve PCEs in the range of 4–8%, with a noticeable decline at lower thicknesses due to limited absorption and unoptimized support layers. In contrast, our optimized structures achieved significantly higher PCEs of 9.39%, 11.25%, 12.70%, and 15.75% for CdTe thicknesses of 100, 150, 200, and 400 nm, respectively—demonstrating the effectiveness of coordinated optimization across all layers. These results confirm that the performance improvements are not solely due to increased absorber thickness but are a direct consequence of simultaneous tuning of the optical and electrical properties of the entire device stack. Therefore, our study presents a substantial departure from traditional CdTe-only optimization methods by introducing a DQL-driven, full-layer optimization strategy that is quantitatively and qualitatively distinct from earlier literature.

In addition to all these evaluations, EQE analysis plays a critical role in comprehensively assessing the optical and electrical performance of photovoltaic devices. EQE represents the efficiency with which the device converts incident photons into electrical

2367198x, 0, Downloaded from https://onlinelibrary.wiley.com/doi/10.1002/solr.202500455 by Cagla Cetinkaya - Istanbul University , Wiley Online Library on [02/09/2025]. See the Terms and Conditions (https://onlinelibrary.wiley.com/terms-and-conditions) on Wiley Online Library for rules of use; OA articles are governed by the applicable Creative Commons License

carriers as a function of wavelength. This enables a detailed examination of how factors such as active layer thickness, the transmittance and absorption characteristics of optical window layers, and other structural elements affect device performance. The analysis provides insight into the wavelength-dependent photon absorption and carrier generation capabilities of the structures incorporating optimized ultra-thin CdTe active layer thicknesses. Within the scope of this study, EQE spectra were computed for ultra-thin CdTe-based solar cells optimized using the DQL algorithm, enabling an evaluation of the optical–photovoltaic integration efficiency of the proposed devices. As shown in Figure 7, the EQE spectra clearly demonstrate the wavelength-dependent photon harvesting efficiency of each optimized structure and its direct contribution to J_{sc} performance.

Figure 7 shows that the EQE values for optimal ultra-thin CdTe-based solar cells exhibit an increasing trend as the active layer thickness increases; this directly demonstrates the dependance of the optical absorption capacity on the active layer thickness and its compatibility with optimized optical absorption spectra. In the 300–500 nm range, all structures exhibit similarly high EQE (approximately 70–80%), corresponding to the spectral region where the SnO_2 and CdS layers function as optical window layers, directing short-wavelength photons to the active layer. The high performance in this region is attributed to the optimized transmittance of the SnO_2/CdS layers, as also observed in the absorption spectra. In the 500–800 nm range, EQEs increase significantly with active layer thickness. While the SC-400 reaches a maximum EQE of approximately 85%, the SC-100 remains at around 65%. This behavior is associated with enhanced optical absorption and increased carrier generation profile enabled by thicker active layers, as discussed in the band diagram analysis. Notably, it was observed that the width and intensity of the optical absorption spectra increased with the increase in the active layer thickness in the p-CdTe layer; this finding is in perfect agreement with the EQE curves.

The band diagram analysis revealed that all optimized structures exhibit a consistent band alignment, with no adverse effects such as tunneling observed in carrier transport. This well-aligned band structure supports efficient carrier collection, thereby contributing to the stabilization of EQEs. In particular, the high EQE observed in the SC-400 indicates the absence of losses due to tunneling or recombination, demonstrating that the optimized MoO_3 and Au layers enhance carrier injection and collection processes, thereby ensuring wavelength-dependent efficiency.

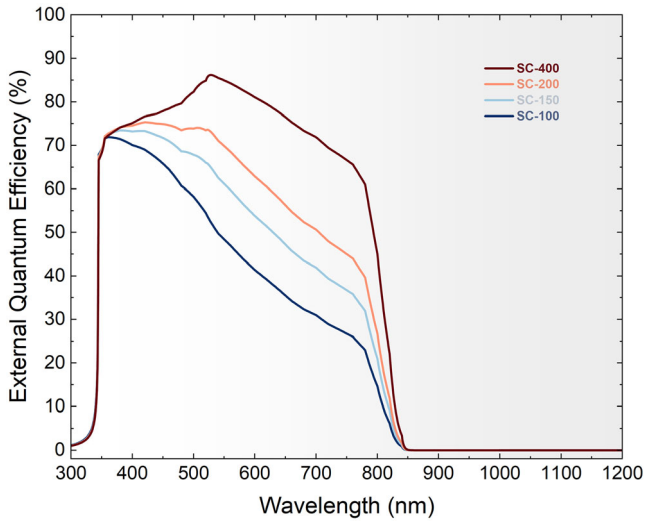


FIGURE 7 | EQE spectra of the optimal ultra-thin CdTe-based solar cells calculated using SCAPS-1D.

The upward trend observed in the EQE spectra is consistent with the J_{sc}'s calculated using SCAPS-1D. While J_{sc} is 11.83 mA/cm^2 in the SC-100, this value increases to 20.86 mA/cm^2 in the SC-400. This increase highlights how the wavelength-dependent performance, as represented in the EQE curves, is effectively optimized with the active layer thickness. Furthermore, the proportional increase in PCE values—from 9.39% for SC-100 to 15.75% for SC-400—corroborates the EQE analysis. In conclusion, the EQE spectra obtained for the DQL-optimized ultra-thin CdTe-based solar cells clearly demonstrate how the DQL algorithm holistically optimizes the optical and electrical parameters through its proposed layer thicknesses. The fact that even the SC-100 with a 100 nm active layer exhibits relatively high EQE values indicates that the optimization of optical window layers (SnO_2/CdS) effectively enhances photon transmission, while the MoO_3/Au layers improve internal reflection and carrier injection. These findings confirm that high photon harvesting and device efficiency are achievable even at ultra-thin active layer thicknesses and that the DQL-based optimization elevates the overall performance by optimizing not only the active layer but all layers in the device architecture.

The optimization framework developed in this study is not limited to CdTe-based solar cells. Its structure is modular and generalizable, making it compatible with other thin-film photovoltaic technologies such as perovskites, CIGS, and organic solar cells, all of which share layer-by-layer architectures. The transition to different materials would require only the substitution of physical models and material parameters (e.g., optical constants, transport characteristics), while the state space could be redefined accordingly.

Furthermore, the methodology applies to other multilayer optoelectronic devices, including light-emitting diodes (LEDs) and lasers. In such cases, the reward function would no longer be based on J_{ph}, but rather on parameters such as radiative intensity, emission wavelength, or the full width at half maximum (FWHM). Similarly, in photonic crystal structures, geometric properties (e.g., periodicity, FF) could be defined as tunable parameters within the state space, enabling optimization for specific photonic bandgap characteristics. This demonstrates that the DQL-based framework is not only effective in photovoltaics but also holds potential for broader applications in photonics and optoelectronic device engineering.

4 | Conclusion

In this study, a novel DQL-based ML framework was developed for the design and optimization of solar cells incorporating

2367198x, 0, Downloaded from https://onlinelibrary.wiley.com/doi/10.1002/solr.202500455 by Cagla Cetinkaya - Istanbul University , Wiley Online Library on [02/09/2025]. See the Terms and Conditions (https://onlinelibrary.wiley.com/terms-and-conditions) on Wiley Online Library for rules of use; OA articles are governed by the applicable Creative Commons License

ultra-thin CdTe active layers. Solar cells with the FTO/SnO_2/CdS/CdTe/MoO_3/Au architecture were thoroughly investigated with a focus on achieving ultra-thin active layers (<400 nm). This investigation was carried out through a comprehensive integration of optical modeling using the TMM and photovoltaic performance analysis using SCAPS-1D simulations.

The primary contributions of this work include the implementation of a RL algorithm to perform full-stack thickness optimization, the demonstration of performance retention at absorber thicknesses as low as 100 nm, and the integration of optical-electrical modeling for AI-guided photovoltaic design. The DQL algorithm has successfully maximized photon harvesting and device efficiency by simultaneously optimizing not only the active layer thicknesses but also the thicknesses of all functional layers (SnO_2, CdS, MoO_3, and Au) in the device. As a result, even for structures incorporating an ultra-thin 100 nm CdTe active layer, a PCE of 9.39% was achieved. This finding demonstrates that ultra-thin architectures, which are typically associated with low efficiency due to limited photon absorption in the literature, can attain high performance through holistic optimization of layer thicknesses and optical-electrical parameters.

The results obtained in this study demonstrate that adjusting the Au layer thickness to 40 nm effectively enhanced internal optical reflection within the device, thereby facilitating photon recycling in the active layer and leading to increased J_{ph}'s. Additionally, the V_{oc}'s remained consistent, ranging from 0.927 to 0.977 V across all structures, indicating that the optimized band alignment was preserved in each case and that efficient carrier transport was achieved. The absence of tunneling effects further confirms that diffusion and drift mechanisms contributed positively to overall device performance.

The optical absorption spectra obtained via TMM and the band diagrams simulated using SCAPS-1D clearly demonstrate how the DQL algorithm holistically optimized both optical and electrical parameters. The increase in J_{sc} with the increasing active layer thickness shows strong agreement with the optimized optical absorption spectra and EQE analyses, confirming the effectiveness of the integrated optimization approach.

Overall, the study highlights the potential of ML, specifically DQL, as an effective exploration tool in high-dimensional, nonlinear design spaces. It emphasizes the critical importance of integrating all layer thicknesses to achieve optimal performance in ultra-thin CdTe solar cells. Through this approach, significant advancements can be made toward reducing material consumption, lowering device weight, and achieving high-efficiency targets, thereby offering a promising roadmap for the development of next-generation flexible and cost-effective photovoltaic technologies.

This approach not only advances the computational design of photovoltaic devices but also offers a scalable strategy for guiding experimental efforts toward lightweight, efficient, and material-conscious solar technologies. Through this approach, significant advancements can be made toward reducing material consumption, lowering device weight, and achieving high-efficiency targets, thereby offering a promising roadmap for the development of next-generation flexible and cost-effective photovoltaic technologies.

Acknowledgments

This work was supported by the Istanbul University Scientific Research Project Coordination Unit (project no: FAB-2023−39931). The authors are grateful for the development and permission to use the SCAPS-1D program from Prof. Marc Burgelman and the group from the University of Ghent, Belgium. We would like to thank Muhammed Yusuf Aykut for his contributions to the coding of algorithms used in AI calculations.

Conflicts of Interest

The authors declare no conflicts of interest.

Data Availability Statement

The data that support the findings of this study are available from the corresponding author upon reasonable request.

References

1. I. Jena and U. P. Singh, *Energy Technology* 13 (2025): 13.

2. R. S. Sutton and A. G. Barto, Reinforcement Learning : An Introduction (MIT Press, 2020).

3. I. Malkiel, M. Mrejen, A. Nagler, U. Arieli, L. Wolf, and H. Suchowski, *Light, Science & Applications* 7 (2018): 60.

4. D. Liu, Y. Tan, E. Khoram, and Z. Yu, *ACS Photonics* 5 (2018): 1365.

5. J. Peurifoy, Y. Shen, L. Jing, et al., *Science Advances* 4 (2018): 4206.

6. Y. Jiang, C. Yao, Y. Yang, and J. Wang, *Solar RRL* 8 (2024): 2400567.

7. J. Peurifoy, Y. Shen, L. Jing, et al., *Science Advances* 4 (2018): eaar4206.

8. F. Li, X. Peng, Z. Wang, et al., *Energy and Environmental Materials* 2 (2019): 280.

9. N. K. Bansal, S. Mishra, H. Dixit, S. Porwal, P. Singh, and T. Singh, *Machine Learning in Perovskite Solar Cells: Recent Developments and Future Perspectives* (John Wiley and Sons Inc, 2023), Vol. 100.

10. S. Mishra, P. Kumar, S. Dey, P. Pattanayak, and T. Singh, *Journal of Environmental Chemical Engineering* 13 (2025): 115260.

11. T. M. Khan, B. Islam, and S. R. Al Ahmed, *Materials Today Communications* 41 (2024): 110490.

12. Y. Liu, W. Yan, S. Han, et al.*Solar RRL* 6 (2022): 2101100.

13. S. Mishra, S. B. Gaikwad, and T. Singh, *Advanced Theory and Simulations* 7 (2024): 2301193.

14. A. I. Shimul, M. A. Khan, A. Rayhan, and A. Ghosh, *Advanced Theory and Simulations* 7 (2025): 2301193.

15. I. Sajedian, H. Lee, and J. Rho, *Solar Energy* 195 (2020): 670.

16. A. Jiang, Y. Osamu, and L. Chen, *Scientific Reports* 10 (2020): 12780.

17. E. Cokduygulular, M. Y. Aykut, and C. Cetinkaya, *Advanced Theory and Simulations* (2025): 2500334.

18. C. Cetinkaya, E. Cokduygulular, M. Y. Aykut, O. Erkal, F. Aydogmus, and B. Kinaci, *Scientific Reports* 15 (2025): 13508.

19. T. Manimozhi, T. Logu, J. Archana, M. Navaneethan, K. Sethuraman, and K. Ramamurthi, *Journal of Materials Science: Materials in Electronics* 31 (2020): 21059.

20. R. Frerichs, *Physical Review* 72 (1947): 594.

21. J. J. Loferski, *Journal of Applied Physics* 27 (1956): 777.

2367198x, 0, Downloaded from https://onlinelibrary.wiley.com/doi/10.1002/solr.202500455 by Cagla Cetinkaya - Istanbul University , Wiley Online Library on [02/09/2025]. See the Terms and Conditions (https://onlinelibrary.wiley.com/terms-and-conditions) on Wiley Online Library for rules of use; OA articles are governed by the applicable Creative Commons License

22. D. Bonnet and H. Rabenhorst, in Photovoltaic Specialists Conference, (9th, Silver Spring, Md, 1972), 129–132.

23. R. Mallick, X. Li, C. Reich, et al., *Ieee Journal of Photovoltaics* 13 (2023): 510.

24. M. Powalla, S. Paetel, E. Ahlswede, R. Wuerz, C. D. Wessendorf, and T. Magorian Friedlmeier, *Applied Physics Reviews* 5 (2018): 041602.

25. Y. Tai, X. Zhang, J. Li, et al., *Renewable and Sustainable Energy Reviews* 207 (2025): 114996.

26. A. Feltrin and A. Freundlich, *Renewable Energy* 33 (2008): 180.

27. M. A. Scarpulla, B. McCandless, A. B. Phillips, et al., *Solar Energy Materials and Solar Cells* 255 (2023): 112289.

28. K. Zweibel, *Solar Energy Materials and Solar Cells* 63 (2000): 375.

29. W. L. Rance, J. M. Burst, D. M. Meysing, et al., *Applied Physics Letters* 104 (2014): 143903.

30. M. Wang, X. Li, and D. Wang, *The European Physical Journal Applied Physics* 83 (2018): 20101.

31. N. Amin, T. Isaka, A. Yamada, and M. Konagai, *Solar Energy Materials and Solar Cells* 67 (2001): 195.

32. L. A. Kosyachenko, X. Mathew, V. Ya Roshko, and E. V. Grushko, *Solar Energy Materials and Solar Cells* 114 (2013): 179.

33. N. R. Paudel, K. A. Wieland, and A. D. Compaan, *Solar Energy Materials and Solar Cells* 105 (2012): 109.

34. A. Gupta, V. Parikh, and A. D. Compaan, *Solar Energy Materials and Solar Cells* 90 (2006): 2263.

35. N. R. Paudel, K. A. Wieland, M. Young, S. Asher, and A. D. Compaan, *Progress in Photovoltaics: Research and Applications* 22 (2014): 107.

36. J. Jasieniak, B. I. MacDonald, S. E. Watkins, and P. Mulvaney, *Nano Letters* 11 (2011): 2856.

37. V. V. Plotnikov, C. W. Carter, J. M. Stayancho, et al., 2013 IEEE 39th Photovoltaic Specialists Conference (PVSC), (IEEE, 2013), 405–408.

38. S. Chander and M. S. Dhaka, *Thin Solid Films* 638 (2017): 179.

39. M. K. S. Bin Rafiq, N. Amin, H. F. Alharbi, et al., *Scientific Reports* 10 (2020): 771.

40. J. Enríquez, *Solar Energy Materials and Solar Cells* 76 (2003): 313.

41. Y. Li, Y.-L. Song, F.-Q. Zhou, et al., *Materials Letters* 164 (2016): 539.

42. F. He, X. Yin, J. Li, et al., *Vacuum* 176 (2020): 109337.

43. M. Cui, A. Lv, and Z. Ma, *Chemphyschem* 23 (2022): e202200091.

44. D.-T. Nguyen, S. Vedraine, L. Cattin, et al., *Journal of Applied Physics* 112 (2012): 063505.

45. F. Li, C. Chen, F. Tan, et al., *Nanoscale Research Letters* 9 (2014): 579.

46. Z. Wang, C. Zhang, R. Gao, et al., *Solar Energy Materials and Solar Cells* 127 (2014): 193.

47. Ç. Çetinkaya, E. Çokduygulular, F. Güzelçimen, and B. Kınacı, *Scientific Reports* 12 (2022): 8822.

48. Ç. Çetinkaya, E. Çokduygulular, B. Kınacı, et al., *Scientific Reports* 12 (2022): 11245.

49. Ç. Çetinkaya, E. Çokduygulular, B. Kınacı, S. Emik, N. A. Sönmez, and S. Özçelik, *Scientific Reports* 12 (2022): 19400.

50. E. Çokduygulular, Ç. Çetinkaya, S. Emik, and B. Kınacı, *Scientific Reports* 13 (2023): 7548.

51. Ç. Çetinkaya, *Optical Materials* 133 (2022): 113003.

52. M. Burgelman, P. Nollet, and S. Degrave, *Thin Solid Films* 361 (2000): 527.

53. B. Mozafari and A. Shahhoseini, *Signal Processing and Renewable Energy* 3 (2020): 57.

54. V. Shukla and G. Panda, *Materials Today Proceedings* 26 (2020): 487.

55. A. Sahoo and S. Mangal, Materials Today: Proceedings (2023), https://doi.org/10.1016/j.matpr.2023.06.109.

56. C.-H. Huang and W.-J. Chuang, *Vacuum* 118 (2015): 32.

57. M. S. Uddin, M. K. Hossain, M. B. Uddin, et al., *Advanced Electronic Materials* 10 (2024): 2300751.

58. A. Ait Abdelkadir, M. Sahal, E. Oublal, Y. Belkassmi, L. El Maimouni, and A. Kotri, *Journal of Materials Research* 38 (2023): 4420.

59. E. Cokduygulular, C. Cetinkaya, S. Emik, and B. Kinaci, *Scientific Reports* 14 (2024): 23430.

60. E. Çokduygulular, Ç. Çetinkaya, S. Emik, and B. Kınacı, *Scientific Reports* 14 (2024): 25679.

61. Ç. Çetinkaya, E. Çokduygulular, B. Kınacı, et al., *Scientific Reports* 11 (2021): 13079.

62. Y. Jin, *Soft Computing* 9 (2005): 3.

63. Y. Bengio, A. Lodi, and A. Prouvost, *European Journal of Operational Research* 290 (2021): 405.

64. T. Hu, B. Luo, and C. Yang, *Discover Artificial Intelligence* 1 (2021): 11.

65. V. Mnih, K. Kavukcuoglu, D. Silver, et al., *Nature* 518 (2015): 529.

66. G.-G. Wang, A. H. Gandomi, A. H. Alavi, and S. Deb, *Neural Computing & Applications* 27 (2016): 989.

67. J. Gong, Y. Cui, F. Li, and M. Liu, *Small Science* 3 (2023): 2200108.

68. Y. Li, W. Yin, R. Deng, et al., *NPG Asia Materials* 4 (2012): e30.

69. Z. Huang, J. Zhu, Y. Hu, et al., *Nanomaterials* 12 (2022): 632.

70. A. Sivaprakasam and N. K. Elangovan, *Journal of Materials Science: Materials in Electronics* 32 (2021): 17612.

2367198x, 0, Downloaded from https://onlinelibrary.wiley.com/doi/10.1002/solr.202500455 by Caglar Cetinkaya - Istanbul University , Wiley Online Library on [02/09/2025]. See the Terms and Conditions (https://onlinelibrary.wiley.com/terms-and-conditions) on Wiley Online Library for rules of use; OA articles are governed by the applicable Creative Commons License